Chapter 5

Neuroelectronics

5.1 Introduction

Neurons are highly specialized for generating and transmitting electrical signals, and for producing electrical signals from chemical inputs. Some important morphological specializations can be seen in the drawings of neurons by Ramón y Cajal shown in figure 5.1; the dendrites that receive inputs from other neurons and the axon that carries the neuronal output to other cells. The elaborate branching structure of the dendritic tree allows a neuron to receive inputs from many other neurons through synaptic connections. The cortical pyramidal neuron of figure 5.1A and the cortical interneuron of figure 5.1C each receive around 10,000 synaptic inputs, and for the cerebellar Purkinje cell of figure 5.1B the number is well over 100,000. Figure 5.1 does not show the full extent of the axons of these neurons. Axons from single neurons can traverse large fractions of the brain or, in some cases, of the entire body. The cell bodies of cortical neurons range in diameter from about 10 to 50 μm. In the mouse brain, where detailed anatomical studies have been done by Braitenberg and Schuz (1991), it has been estimated that cortical neurons typically send out a total of about 40 mm of axon and have around 4 mm of total dendritic cable in their branched dendritic trees. The axon makes an average of 180 synaptic connections with other neurons per mm of length while the dendritic tree receives, on average, 2 synaptic inputs per μm.

Along with these morphological features, neurons have physiological specializations. Most prominent among these are a wide variety of membrane channels that control the movement of ions, predominantly sodium, Na^+, potassium, K^+, calcium, Ca^{2+}, and chloride, Cl^-, into and out of the cell. The electrical signal of relevance to the nervous system is the difference in electrical potential between the interior of a neuron and the surrounding extracellular medium. Under resting conditions, the potential inside the cell membrane of a neuron is about -70 mV relative to that of the sur-

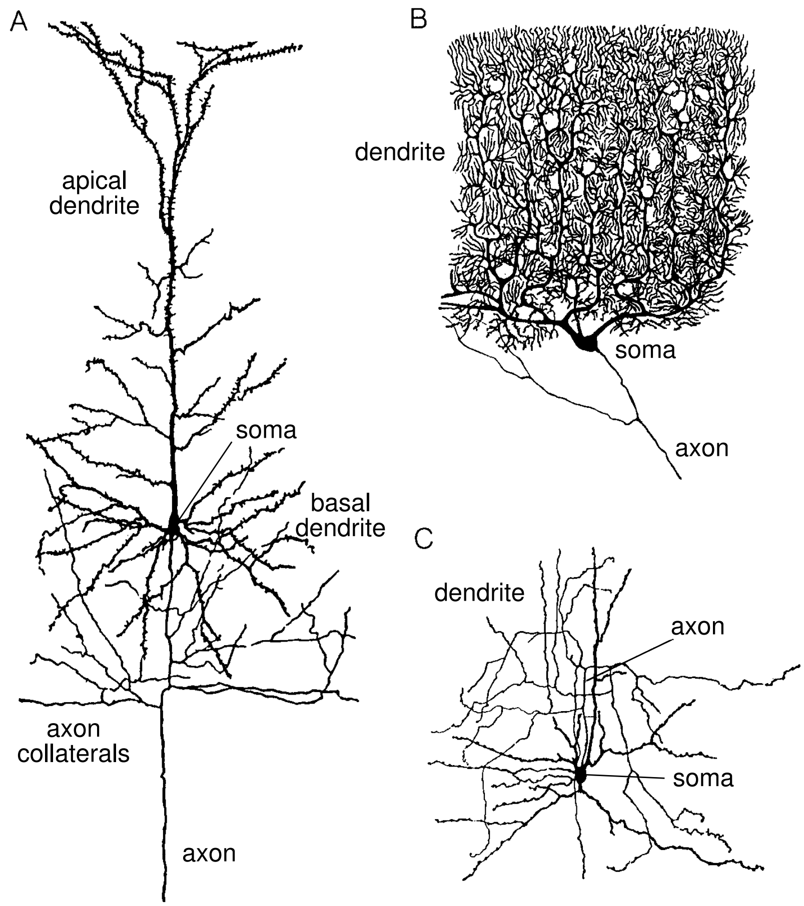

Figure 5.1: Diagrams of three neurons. A) A cortical pyramidal cell. These are the primary excitatory signaling neurons of the cerebral cortex. Pyramidal cell axons branch locally, sending axon collaterals to synapse with nearby neurons, and also project more distally to conduct signals to other parts of the brain and nervous system. B) A Purkinje cell of the cerebellum. Purkinje cell axons transmit the output of the cerebellar cortex. C) A stellate cell of the cerebral cortex. These neurons are one of a large class of cells that provide inhibitory input to the neurons of the cerebral cortex. To give an idea of scale, these figures are magnified about 150 fold. (Drawings from Cajal, 1911; figure from Dowling, 1992)

rounding bath (which is conventionally defined to be 0 mV), and the cell is said to be polarized. Ion pumps located in the cell membrane maintain concentration gradients that support this membrane potential difference. For example, Na^+ is about 10 times more concentrated outside a neuron than inside it, and the concentration of K^+ is about 50 times higher inside the neuron than in the extracellular medium. Channels control the flow of ions across the cell membrane by opening and closing in response to voltage changes and both internal and external molecular signals. Current, in the form of charged ions, flowing out of the cell through open channels makes the membrane potential more negative, hyperpolarizing the cell. Current flowing into the cell changes the membrane potential to less negative or even positive values, a process known as depolarization.

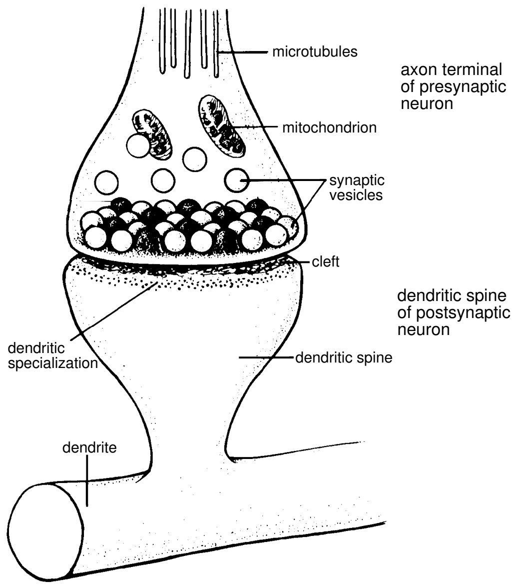

Figure 5.2: Diagram of a synapse. The axon terminal or bouton is at the end of the axonal branch seen entering from the top of the figure. It is filled with synaptic vesicles containing the neurotransmitter that is released when an action potential arrives from the presynaptic neuron. Transmitter crosses the synaptic cleft and binds to receptors on the dendritic spine, a roughly one μm long process extending from the dendrite of the postsynaptic neuron. Excitatory synapses onto pyramidal cells in the brain form on dendritic spines as shown here. Other synapses form directly on the dendrites, axon, or soma of the postsynaptic neuron. (Adapted from Kandel and Schwartz, 1985.)

A variety of transduction mechanisms in sensory receptor neurons cause ion channels to open or close in response to the relevant stimulus; light, sound or pressure, for example. The resulting change in the balance of charge modifies the membrane potential, producing an electrical signal related to the stimulus. This signal typically leads to the generation of a sequence of action potentials that propagate along axon processes. Axons terminate at synapses where the voltage transient of the action potential opens ion channels producing an influx of Ca^{2+} that leads to the release of a neurotransmitter (figure 5.2). The neurotransmitter binds to receptors at the signal receiving or postsynaptic side of the synapse causing ion-conducting channels to open. Depending on the nature of the ion flow, the synapses can have either an excitatory, depolarizing, or an inhibitory, typically hyperpolarizing, effect on the postsynaptic neuron. A similar process at the neuromuscular junction causes Ca^{2+} influx into muscle fibers leading to contraction.

Many of membrane and synaptic currents that effect neuronal activity can be described mathematically with considerable precision. The construction of model neurons and various simplifications used to streamline neuronal modeling are discussed in chapter 6. Circuits and networks of model neurons are studied in chapter 7. In this chapter, we discuss the electrical properties of neurons and synapses and develop the mathematical descriptions upon which neuronal and network modeling are based.

5.2 Electrical Properties of Neurons

Like other cells, neurons are packed with a huge number and variety of ions and molecules. A cubic micron of cytoplasm might contain, for example, 10^{10} water molecules, 10^8 ions, 10^7 small molecules such as amino acids and nucleotides, 10^5 proteins, and 10^5 RNA molecules. Many of these molecules carry charges, either positive or negative. Most of the time, there is an excess concentration of negative charge inside a neuron. Excess charges that are mobile, like ions, repel each other and build up on the inside surface of the cell membrane. Electrostatic forces attract an equal density of positive ions from the extracellular medium to the outside surface of the membrane.

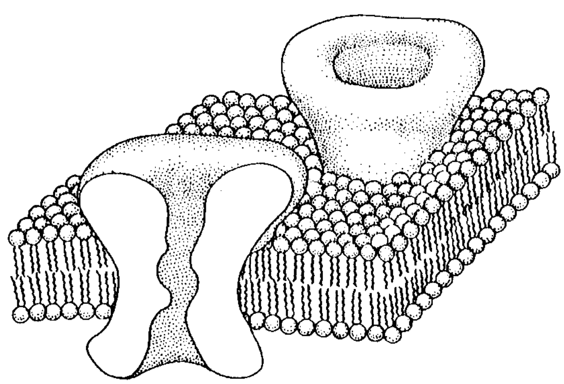

Figure 5.3: A schematic diagram of a section of the lipid bilayer that forms the cell membrane with two ion channels embedded in it. The membrane is 3 to 4 nm thick and the ion channels are about 10 nm long. (From Hille, 1992)

The cell membrane is a lipid bilayer 3 to 4 nm thick that is essentially impermeable to most charged molecules. This insulating feature causes the cell membrane to act as a capacitor by separating the charges lying along its interior and exterior surfaces. Numerous ion conducting channels embedded in the cell membrane (figure 5.3) lower the membrane resistance for ion flow to a value about 10,000 times smaller than that of a pure lipid bilayer. This gives the membrane a non-zero conductance that varies depending on the state of the ion channels. A typical neuron may have a dozen or more different types of channels, anywhere from a few to hundreds of channels in a square micron of membrane, and hundreds of thousands to millions of channels in all. Many, but not all, channels are highly selective, allowing only a single type of ion to pass through them (to an accuracy of about 1 ion in 10^4).

By convention, the potential of the extracellular fluid outside a neuron is defined to be zero. When a neuron is inactive, an excess of internal negative charge causes the potential inside the cell membrane to be about -70 mV. This potential is an equilibrium point at which the flow of ions into the cell matches that out of the cell. The potential can change if the balance of ion flow is modified by the opening or closing of ion channels. Under normal conditions, neuronal membrane potentials vary over a range from about -90 to +50 mV. The order of magnitude of these potentials can be estimated from basic physical principles. Membrane potentials are small enough to allow neurons to take advantage of thermal energy to help transport ions across the membrane, but are large enough so that thermal fluctuations do not swamp the signaling capabilities of the neuron. These conditions imply that potential differences across the cell membrane must lie in a range so that the energy gained or lost by an ion traversing the membrane is the same order of magnitude as the thermal energy of that ion. The thermal energy of an ion is about $k_\mathrm{B}T$ where k_B is the Boltzmann constant and T is the temperature on an absolute Kelvin scale. For chemists and biologists (though not for physicists), it is more customary to discuss moles of ions rather than single ions. A mole of ions has Avagadro's number times as much thermal energy as a single ion, or RT, where R is the universal gas constant equal to 8.31 joules/mol K$^\circ$ = 1.98 cal/mol K$^\circ$. RT is about 2500 joules/mol or 0.6 kCal/mol at normal temperatures. To estimate the size of typical membrane potentials, we equate this to the energy gained or lost when a mole of ions crosses a membrane with a potential difference V_T across it. This energy is FV_T where F is the Faraday constant, F = 96,480 Coulombs/mol, equal to Avagadro's number times the charge of a single proton, q. Setting $FV_T = RT$ gives

$$V_T = \frac{RT}{F} = \frac{k_\mathrm{B}T}{q} \, . \tag{5.1}$$

This is an important parameter that enters into a number of calculations. V_T is between 24 and 27 mV for the typical temperatures of cold and warm-blooded animals. This sets the overall scale for membrane potentials across neuronal membranes.

The voltage across the membrane and the amount of excess charge Q inside the membrane for a region such as that shown in figure 5.4 are related

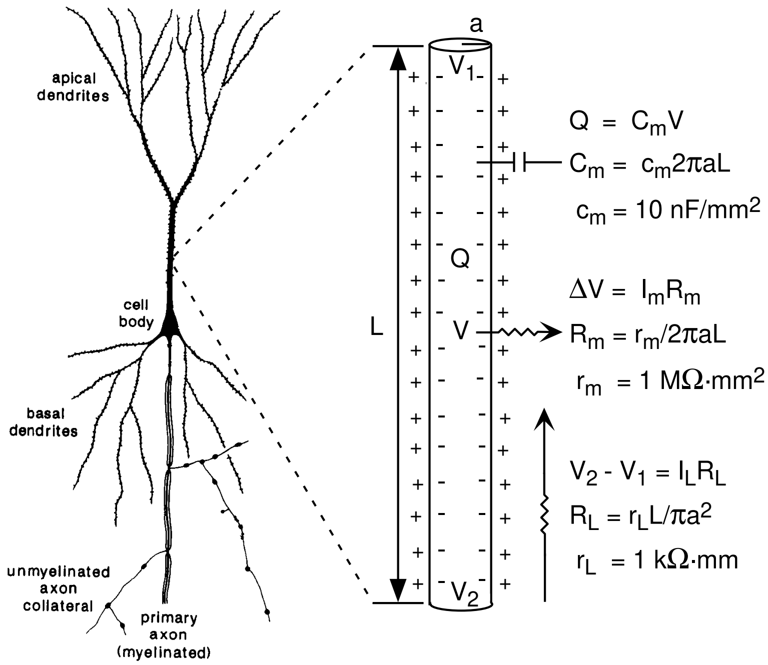

Figure 5.4: The capacitance, membrane resistance, and longitudinal resistance of a piece of a dendrite. A cylindrical segment of the apical dendritic shaft of length L and radius a is shown in the expanded view. Equations discussed in the text are summarized at the right. Typical values of c_{m}, r_{m}, and r_{L} are given, but values may vary for different neurons, and, in the case of the membrane resistance, at different times. (Neuron diagram from Haberly, 1990)

by the standard equation for a capacitor, $Q = C_{\mathrm{m}}V$. Here V is the intracellular or membrane potential, and C_{m} is the membrane capacitance of the region being considered. The membrane capacitance is proportional to the amount of membrane or, equivalently, to the surface area of the region. The constant of proportionality, called the specific membrane capacitance, is the capacitance per unit area of membrane and is approximately the same for all neurons, $c_{\mathrm{m}} = 10\ \mathrm{nF/mm^2}$ (values in the range of 10 to 20 $\mathrm{nF/mm^2}$ are typically reported). The total capacitance C_{m} is the membrane surface area times the specific capacitance c_{m}. For the cylindrical region drawn in the expanded view in figure 5.4, the surface area is the length times the circumference, $2\pi aL$, so the capacitance of this region is $C_{\mathrm{m}} = 2\pi aLc_{\mathrm{m}}$.

The specific membrane capacitance can also be used to determine the capacitance of an entire neuron. Neuronal surface areas tend to be in the range 0.01 to 0.1 $\mathrm{mm^2}$ so the membrane capacitance for a whole neuron is typically 0.1 to 1 nF. For a neuron with a total membrane capacitance of 1 nF, 7×10^{-11} C or about a billion singly charged ions are required to produce a resting potential of -70 mV. This is about a hundred-thousandth of the total number of ions in a neuron and is the amount of charge delivered by a 0.7 nA current in 100 ms. We can use the membrane capacitance to determine how much current is required to change the membrane potential at a given rate. The time derivative of the basic equation relating the membrane potential and charge,

$$C_{\mathrm{m}} \frac{dV}{dt} = \frac{dQ}{dt}\,, \tag{5.2}$$

plays an important role in the mathematical modeling of neurons. The time derivative of the charge dQ/dt is equal to the current passing into the cell, so the amount of current needed to change the membrane potential of a neuron with a total capacitance C_{m} at a rate dV/dt is $C_{\mathrm{m}} dV/dt$. For example, 1 nA will change the membrane potential of a neuron with a capacitance of 1 nF at a rate of 1 mV/ms.

The capacitance of a neuron determines how much current is required to make the membrane potential change at a given rate. Holding the membrane potential at a steady value different from the membrane potential of the neuron also requires current, but this current is determined by the membrane resistance rather than by the capacitance of the cell. The net amount of current I_{m} that leaves the cell when the membrane potential is shifted by an amount ΔV away from its resting value is given in terms of the membrane resistance R_{m} by Ohm's law, $\Delta V = I_{\mathrm{m}} R_{\mathrm{m}}$. Because membrane resistances are voltage-dependent, this law only applies for small values of ΔV. The membrane resistance is the inverse of the membrane conductance, and, like the capacitance, the conductance of a piece of cell membrane is proportional to its surface area. Conversely, the membrane resistance R_{m} is equal to the specific membrane resistance r_{m} divided by the surface area. A typical value for the specific membrane resistance when a neuron is in a resting state is around 1 MΩ·mm^2. This number is much more variable than the specific membrane capacitance. Membrane resistances vary considerably among cells and under different conditions and at different times for a given neuron, depending on the number, type, and state of its ion channels. The membrane resistance of the cylindrical piece of membrane in figure 5.4 is r_{m} divided by the surface area, or $R_{\mathrm{m}} = r_{\mathrm{m}}/2\pi aL$.

The specific membrane resistance of a neuron can vary as a function of time, and may take different values for different regions of the cell's membrane. The membrane resistance of a entire neuron can obtained by dividing the appropriate r_{m} value by the total surface area of membrane. For total surface areas between 0.01 and 0.1 mm, the neuronal membrane (also known as input) resistance is in the range 10 to 100 MΩ. With a 100 MΩ membrane resistance, a steady-state current of 0.1 nA is required to hold change the membrane potential 10 mV away from its resting value.

The product of the membrane capacitance and the membrane resistance is a quantity with the units of time called the membrane time constant, $\tau_{\mathrm{m}} =$

$R_m C_m$. Because C_m and R_m have inverse dependences on the membrane surface area, the membrane time constant is independent of area and equal to the product of the specific membrane capacitance and resistance, $\tau_m = r_m c_m$. The membrane time constant sets the basic time scale for changes in the membrane potential and typically falls in the range between 10 and 100 ms.

Because of the elongated and highly branched structure of most neurons, the membrane potential measured in different parts of a neuron can take different values. Figure 5.5A shows the delay and attenuation of an ac-

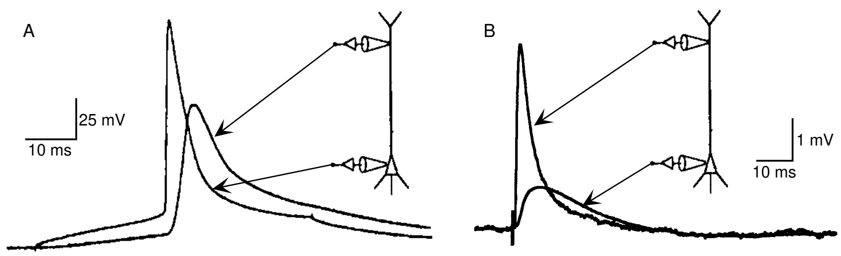

Figure 5.5: Simultaneous intracellular recordings from the soma and apical dendrite of a cortical pyramidal neuron in slice preparations. A) A pulse of current was injected into the soma of the neuron to produce the action potential seen in the somatic recording. The action potential appears delayed and with smaller amplitude in the dendritic recording. B) A set of axon fibers was stimulated producing an excitatory synaptic input. The excitatory postsynaptic potential is larger and peaks earlier in the dendrite than in the soma. Note that the scale for the potential is smaller than in A. (A adapted from Stuart and Sakmann, 1994; B adapted from Stuart and Spruston, 1998)

tion potential as it propagates from the soma out to the dendrites of a cortical pyramidal neuron. Action potentials normally originate near the soma, or cell body, of a neuron and backpropagation of the action potential into the dendrites, as seen in figure 5.5A, is thought to play an important role in activity-dependent processes that modify synaptic strength. Figure 5.5B shows the delay and attenuation of an excitatory postsynaptic potential (EPSP) initiated in the dendrite by synaptic input as it spreads to the soma. Understanding this process is crucial for determining whether a given synaptic input is sufficient to cause a neuron to fire an action potential.

Potential differences between different parts of a neuron cause ions to flow within the cell. The intracellular medium provides a resistance to such flow. The longitudinal current, I_L, flowing within a neuron can be computed from Ohm's law. For the cylindrical segment of dendrite shown in figure 5.4, the longitudinal current flowing from the bottom to the top is determined by $V_2 - V_1 = I_L R_L$. R_L is called the longitudinal resistance. The longitudinal resistance grows in proportion to the length of the segment (long segments have higher resistances than short ones) and is inversely proportional to the cross-sectional area of the segment (thin segments have higher resistances than fat ones). The constant of proportionality is called the intracellular resistivity, r_{L}, and it typically falls in the range from 1 to 3 kΩ·mm. The longitudinal resistance of the segment in figure 5.4 is r_{L} times the length L divided by the cross-sectional area πa^2, $R_{\mathrm{L}} = r_{\mathrm{L}} L/\pi a^2$. A segment 100 μm long with a radius of 2 μm has a longitudinal resistance of about 8 MΩ. A voltage difference of 8 mV would be required to force 1 nA of current down such a segment.

Current flows within a neuron due to voltage gradients. Voltage gradients are greatest along narrow dendritic or axonal cables, and, for such structures, voltage gradients in the longitudinal direction are much greater than those in directions perpendicular to the length of the cable. For this reason, we restrict the discussion to longitunal gradients and current flows. We can relate the longitudinal current to the local voltage gradient at any point within a neuron by considering a short segment of length Δx and radius a. This segment has longitudinal resistance $r_{\mathrm{L}}\Delta x/\pi a^2$. If the voltage difference across the segment is ΔV, the magnitude of the longitudinal current will be this voltage divided by the longitudinal resistance, $\Delta V \pi a^2/r_{\mathrm{L}}\Delta x$. In the limit of very short segment length, $\Delta x \to 0$, the ratio of ΔV to Δx becomes the derivative $\partial V/\partial x$ so that

$$I_{\mathrm{L}} = -\frac{\pi a^2}{r_{\mathrm{L}}}\frac{\partial V}{\partial x} \tag{5.3}$$

(we write the spatial derivative as a partial derivative because V may also depend on time). The current defined by equation 5.3 is positive in the direction of increasing x, and the minus sign indicates that it flows in the direction that opposes the voltage gradient.

We can use the intracellular resistivity to crudely estimate the conductance of a single channel. We approximate the channel pore as a tube of length 6 nm and opening area 0.15 nm^2 (see Hille, 1992). This gives an order of magnitude estimate for the conductance of 0.15 nm $^2/(1$ kΩ mm $\times$ 6 nm) $\approx$ 25 pS, which is the right order of magnitude for a channel conductance.

5.3 The Cable Equation

The dendrites and axons of neurons are composed of long, narrow, branching, tubular cables. For this reason, the problem of computing the membrane potential at different locations within a neuron is known as cable theory. Dendritic and axonal cables are typically narrow enough so that variations of the potential in the radial or axial directions are negligible compared to longitudinal variations. Therefore, the membrane potential along a neuronal cable is expressed as a function of a single longitudinal spatial coordinate x, and the basic problem is to solve for this potential at different times.

The membrane potential $V(x, t)$ is determined by solving a partial differential equation, the cable equation, that describes how the currents entering, leaving, and flowing within a neuron affect the rate of change of the membrane potential. To derive the cable equation, we consider the currents within the small segment shown in figure 5.6. This segment has a radius a and a short length Δx. The rate of change of the membrane potential due to currents flowing into and out of this region is determined by its capacitance. The cylinder of membrane shown in figure 5.6 has a surface area of $2\pi a\Delta x$ and a capacitance of $2\pi a\Delta x c_{\mathrm{m}}$. The amount of current needed to change the membrane potential at a rate $\partial V/\partial t$ is $2\pi a\Delta x c_{\mathrm{m}}\partial V/\partial t$.

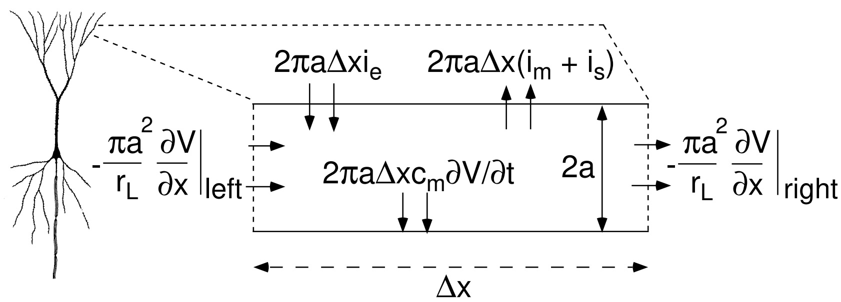

Figure 5.6: The segment of neuron used in the derivation of the cable equation. The longitudinal, membrane, and electrode currents that determine the rate of change of the membrane potential within this segment are denoted. The segment has length Δx and radius a.

All of the currents that can change the membrane potential of the segment being considered are shown in figure 5.6. Current can flow longitudinally into the segment from neighboring segments, and expression 5.3 has been used in figure 5.6 to specify the longitudinal current at both ends of the segment. Current can flow across the membrane of the segment we are considering through ion channels, through synaptic receptor channels, or through an electrode. All three of these contributions are expressed as currents per unit area of membrane times the surface area of the segment, $2\pi a\Delta x$. The membrane current per unit area arising from all but the synaptic channels is denoted by i_{m}, and the synaptic current per unit area is i_{s}. Likewise, i_{e} is the current per unit area of membrane coming from any electrode penetrating the cell. Normally, current flow from an electrode is described by specifying the total current I_{e} not the current per unit area i_{e}. Within the cable equation, it is more convenient to use i_{e} than I_{e}, but when we solve the cable equation, all the results we obtain will be re-expressed in the conventional way in terms of the total electrode current I_{e}. Following the standard convention, membrane and synaptic currents are defined as positive when they are outward, and electrode currents are defined as positive when they are inward.

The cable equation is derived by setting the sum of all the currents shown in figure 5.6 equal to the current needed to charge the membrane. The total longitudinal current entering the cylinder is the difference between the current flowing in on the left and that flowing out on the right. Thus

$$2\pi a \Delta x c_{\mathrm{m}} \frac{\partial V}{\partial t} = -\left(\frac{\pi a^2}{r_{\mathrm{L}}}\frac{\partial V}{\partial x}\right)\bigg|_{\mathrm{left}} + \left(\frac{\pi a^2}{r_{\mathrm{L}}}\frac{\partial V}{\partial x}\right)\bigg|_{\mathrm{right}} - 2\pi a \Delta x (i_{\mathrm{m}} + i_{\mathrm{s}} - i_{\mathrm{e}})\,. \tag{5.4}$$

Ultimately, we are going to take the limit $\Delta x \to 0$, so we note that in this limit

$$\frac{1}{\Delta x}\left[\left(\frac{\pi a^2}{r_{\mathrm{L}}}\frac{\partial V}{\partial x}\right)\bigg|_{\mathrm{right}} - \left(\frac{\pi a^2}{r_{\mathrm{L}}}\frac{\partial V}{\partial x}\right)\bigg|_{\mathrm{left}}\right] \to \frac{\partial}{\partial x}\left(\frac{\pi a^2}{r_{\mathrm{L}}}\frac{\partial V}{\partial x}\right) \tag{5.5}$$

Substituting this into 5.4 after dividing both sides by $2\pi a \Delta x$, we obtain the cable equation

$$c_{\mathrm{m}} \frac{\partial V}{\partial t} = \frac{1}{2 a r_{\mathrm{L}}} \frac{\partial}{\partial x}\left(a^2 \frac{\partial V}{\partial x}\right) - i_{\mathrm{m}} - i_{\mathrm{s}} + i_{\mathrm{e}}\,. \tag{5.6}$$

We have moved r_{L} outside the derivative in this equation under the assumption that it is not a function of position.

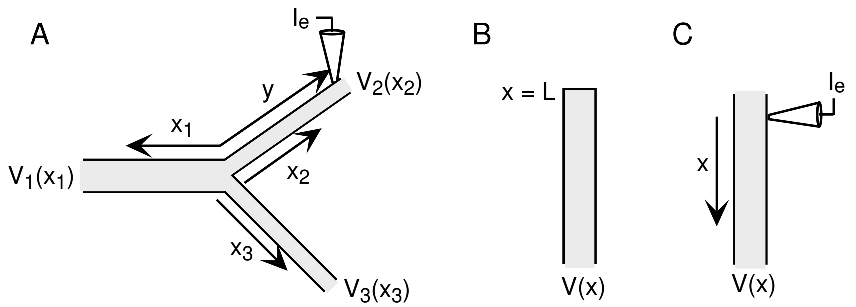

Figure 5.7: Branching nodes, terminals, and an infinite cable. A) A branching node. The three different segments are labeled by indices 1, 2, and 3. The coordinates x_1, x_2, and x_3 measure the distances out from the node to the position where the membrane potential is evaluated on each branch. In this example, current is injected into segment 2 a distance y from the junction. B) The termination of a segment. This segment ends at the point $x = L$. C) An infinite cable. The open ends indicate that this cable extends indefinitely in both directions. In this case, the coordinate x is measured relative to the site of current injection.

To determine the membrane potential, equation (5.6) must be augmented by appropriate boundary conditions. The boundary conditions specify what happens to the membrane potential at locations where the neuronal cable branches or terminates. The node at which a cable branches is treated as a point where multiple cable segments join. At such a branching node (figure 5.7A), the potential V must be continuous, that is, the voltage along each segment must yield the same value when evaluated at the node. In addition, charge must be conserved so the sum of the longitudinal currents entering or leaving a node along all of its branches must be zero. Using the notation of figure 5.7A and equation (5.3) for the longitudinal current, these conditions are $V_1(0) = V_2(0) = V_3(0)$ and

$$a_1^2 \left.\frac{\partial V_1}{\partial x_1}\right|_{x_1=0} + a_2^2 \left.\frac{\partial V_2}{\partial x_2}\right|_{x_2=0} + a_3^2 \left.\frac{\partial V_3}{\partial x_3}\right|_{x_3=0} = 0 \tag{5.7}$$

Several different boundary conditions can be imposed at the end of a terminating cable segment. A reasonable condition is that no current flows out the end of the cable. By equation (5.3) this means that the spatial derivative of the potential must vanish at a termination point. For the example of figure 5.7B, this means that

$$\left.\frac{\partial V}{\partial x}\right|_{x=L} = 0\,. \tag{5.8}$$

Due to the complexities of neuronal membrane currents and morphologies, the cable equation is most often solved numerically using techniques described in chapter 6. However, it is useful to study analytic solutions of the cable equation in simpler cases to get a feel for how different morphological features such as long dendritic cables, branching nodes, changes in cable radius, and cable ends affect the membrane potential.

Linear Cable Theory

Before we can solve the cable equation by any method, the membrane current i_{m} and synaptic current i_{s} must be specified. We discuss detailed models for these currents later in this chapter. These models typically produce expressions that are too complex (*i.e.* nonlinear) to allow analytic solutions of the cable equation. The analytic solutions we discuss use two rather drastic approximations; synaptic currents are ignored ($i_{\mathrm{s}} = 0$), and the membrane current is written as a linear function of the membrane potential. Eliminating synaptic currents requires us to examine how a neuron responds to the injected current i_{e}. In some cases, injected current can mimic the effects of a synaptic conductance, although the two are not equivalent. Nevertheless, studying responses to injected current allows us to investigate the effects of different morphologies on membrane potentials.

Typically, a linear approximation for the membrane current is only valid if the membrane potential stays within a limited range, for example close to the resting potential of the cell. The resting potential is defined as the potential where no net current flows across the membrane. Near this potential, we approximate the membrane current per unit area as

$$i_{\mathrm{m}} = (V - V_{\mathrm{rest}})/r_{\mathrm{m}} \tag{5.9}$$

where V_{rest} is the resting potential, and the factor of r_{m} follows from the definition of the membrane resistance. It is convenient to define v as the membrane potential relative to the resting potential, $v = V - V_{\rm rest}$, so that $i_{\rm m} = v/r_{\rm m}$.

If the radii of the cable segments used to model a neuron are constant except at branches and abrupt junctions, the factor a^2 in equation 5.6 can be taken out of the derivative and combined with the prefactor $1/2ar_{\rm L}$ to produce a term $a/2r_{\rm L}$ that multiplies the second spatial derivative. With this modification, use of the linear expression for the membrane current, and setting $i_{\rm s} = 0$, the cable equation for v is

$$c_{\rm m}\frac{\partial v}{\partial t} = \frac{a}{2r_{\rm L}}\frac{\partial^2 v}{\partial x^2} - \frac{v}{r_{\rm m}} + i_{\rm e}\,. \tag{5.10}$$

Next, we multiply this equation by $r_{\rm m}$, turning the factor that multiplies the time derivative on the left side into the membrane time constant $\tau_{\rm m} = r_{\rm m}c_{\rm m}$. This also changes the expression multiplying the spatial second derivative on the right side of equation 5.10 to $ar_{\rm m}/2r_{\rm L}$. This factor has the dimensions of length squared, and it defines a fundamental length constant for a segment of cable of radius a, the electrotonic length

$$\lambda = \sqrt{\frac{ar_{\rm m}}{2r_{\rm L}}}\,. \tag{5.11}$$

Expressed in terms of $\tau_{\rm m}$ and λ, the linear cable equation becomes

$$\tau_{\rm m}\frac{\partial v}{\partial t} = \lambda^2\frac{\partial^2 v}{\partial x^2} - v + r_{\rm m}i_{\rm e}\,. \tag{5.12}$$

Equation 5.12 is linear in v and can be solved by standard methods of mathematical analysis (for specific methods, see the references). The constants $\tau_{\rm m}$ and λ set the scale for temporal and spatial variations in the membrane potential. For example, the membrane potential will require a time of order $\tau_{\rm m}$ to settle down after a transient, and deviations in the membrane potential due to localized current injections will typically decay back to zero over a length of order λ.

The membrane potential is affected both by the form of the cable equation and by the boundary conditions imposed at branching nodes and terminations. To isolate these two effects, we consider two idealized cases: an infinite cable that does not branch or terminate (figure 5.7C), and a single branching node that joins three semi-infinite cables (figure 5.7A). Of course, real neuronal cables are not infinitely long, but the solutions we find are applicable for regions of a long cable far from the ends. We will determine the potential for both of these morphologies when current is injected at a single point along the cable at a location y. Because the equation we are studying is linear, any other spatial configuration of injected current can be determined by summing solutions corresponding to current injection at different points. The use of point injection to build more general solutions is a standard method of linear analysis. In this context, the solution for a point source of current injection is called a Green's function.

An Infinite Cable

In general, solutions to the linear cable equation are functions of position and time. However, if the current being injected is held constant, the membrane potential will settle to a steady-state solution that is independent of time. Solving for this time-independent solution is easier than solving the full time-dependent equation, because the cable equation reduces to an ordinary differential equation in the static case, $\lambda^2 d^2 v/dx^2 = v - r_{\mathrm{m}} i_{\mathrm{e}}$. For the localized current injection we wish to study, i_{e} is zero everywhere except within a small region of size Δx around the injection site, which we take to be $x = 0$. Eventually we will let $\Delta x \to 0$. Away from the injection site, the linear cable equation is $\lambda^2 d^2 v/dx^2 = v$, which has the general solution $v(x) = A_1 \exp(-x/\lambda) + A_2 \exp(x/\lambda)$ with as yet undetermined coefficients A_1 and A_2. These constant coefficients are determined by imposing boundary conditions appropriate to the particular morphology being considered. For an infinite cable, we simply require that the solution does not grow without bound when $x \to \pm\infty$ since an infinite value of v is physically impossible. This means that we must choose the solution with $A_1 = 0$ for the region $x < 0$ and the solution with $A_2 = 0$ for $x > 0$. Because the solution must be continuous at $x = 0$, we must require $A_1 = A_2 = A$, and these two solutions can be combined into a single expression $v(x) = A \exp(-|x|/\lambda)$. The remaining task is to determine A.

In the small region of size Δx near $x = 0$ where the current is injected, the full equation $\lambda^2 d^2 v/dx^2 = v - r_{\mathrm{m}} i_{\mathrm{e}}$ must be solved. If the total amount of current injected by the electrode is I_{e}, the current per unit area injected into this region is $I_{\mathrm{e}}/2\pi a \Delta x$. This grows without bound as $\Delta x \to 0$. The membrane potential $v(x) = A \exp(-|x|/\lambda)$ is finite within this region, but its first derivative is discontinuous. For small Δx, the derivative on one side of the region (at $x = -\Delta x/2$) is approximately A/λ, while on the other side (at $x = +\Delta x/2$) it is $-A/\lambda$ (we used the fact that Δx is small to set $\exp(-|\Delta x|/2\lambda) \approx 1$). For small Δx, the second derivative is approximately the difference between these two first derivatives divided by Δx, which is $-2A/\lambda\Delta x$. We can ignore the term v in the cable equation within this small region, because it is not proportional to $1/\Delta x$. Substituting the expressions we have derived for the remaining terms in the equation, we find that $-2\lambda^2 A/\lambda\Delta x = -r_{\mathrm{m}} I_{\mathrm{e}}/2\pi a \Delta x$, so $A = r_{\mathrm{m}} I_{\mathrm{e}}/4\pi a \lambda$. The expression $r_{\mathrm{m}}/2\pi a \lambda$ gives the resistance of a segment of membrane of radius a that is one electrotonic length constant long. This resistance enters into a number of our calculations, and we denote it by

$$R_\lambda = \frac{r_{\mathrm{m}}}{2\pi a \lambda} = \frac{r_{\mathrm{L}} \lambda}{\pi a^2} . \tag{5.13}$$

The second equality can be verified by using expression 5.11 for λ. Equation 5.13 indicates that R_λ is both the membrane resistance and the longitudinal resistance of a cable segment of radius a and length λ (they are equal for this particular segment length).

Using 5.13, we find $A = I_{\mathrm{e}} R_\lambda/2$, and the membrane potential for static current injection at the point $x = 0$ along an infinite cable is

$$v(x) = \frac{I_e R_\lambda}{2} \exp\left(-\frac{|x|}{\lambda}\right) . \tag{5.14}$$

The value of the potential at $x = 0$ is $I_e R_\lambda/2$ indicating that the infinite cable has an input resistance of $R_\lambda/2$. Each direction of the cable acts like a resistance of R_λ and these two act in parallel to produce a total resistance half as big. Note that each semi-infinite cable extending from the point $x = 0$ has a resistance equal to a finite cable of length λ. As seen in figure 5.8A, the membrane potential away from the site of current injection ($x = 0$) decays exponentially with length constant λ.

We now consider the membrane potential produced by an instantaneous pulse of current injected at the point $x = 0$ at the time $t = 0$. Specifically, we consider $i_e = I_e\delta(x)\delta(t)/2\pi a$. We will not derive the solution for this case (see for example Tuckwell, 1988), but simply state the answer

$$v(x, t) = \frac{I_e R_\lambda}{\sqrt{4\pi\lambda^2 t/\tau_m}} \exp\left(-\frac{\tau_m x^2}{4\lambda^2 t}\right) \exp\left(-\frac{t}{\tau_m}\right) . \tag{5.15}$$

In this case, the spatial dependence of the potential is determined by a Gaussian, rather than an exponential function. The Gaussian is always centered around the injection site, so the potential is always largest at $x = 0$. The width of the Gaussian curve around $x = 0$ is proportional to $\lambda\sqrt{t/\tau_m}$. As expected, λ sets the scale for this spatial variation, but the width also grows as the square root of the time measured in units of τ_m. The factor $(4\pi\lambda^2 t/\tau_m)^{-1/2}$ in equation 5.15 preserves the total area under this Gaussian curve, but the additional exponential factor $\exp(-t/\tau_m)$ reduces the integrated amplitude over time. As a result, the spatial dependence of the membrane potential is described by a spreading Gaussian function with an integral that decays exponentially (figure 5.8B).

Figure 5.9 illustrates the properties of the solution 5.15 plotted as a function of time. Figure 5.9A shows that the membrane potential measured further from the injection site reaches its maximum value at later times. It is important to keep in mind that the membrane potential spreads out from the region $x = 0$, it does not propagate like a wave. Nevertheless, we can define a type of 'velocity' for this solution by computing the time t_{max} when the maximum of the potential occurs as a function of time at a given spatial location. This is done by setting the derivative of $v(x, t)$ with respect to t to zero, giving

$$t_{max} = \frac{\tau_m}{4}\left(\sqrt{1 + 4(x/\lambda)^2} - 1\right) . \tag{5.16}$$

For large x, $t_{max} \approx x\tau_m/2\lambda$ corresponding to a velocity of $2\lambda/\tau_m$. For smaller x values, the location of the maximum moves faster than this 'velocity' would imply (figure 5.9B).

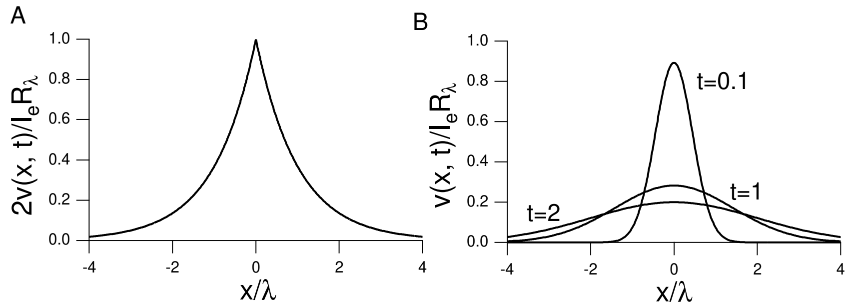

Figure 5.8: The potential for current injection at the point $x = 0$ along an infinite cable. A) Static solution for a constant current. The potential decays exponentially away from the site of current injection. B) Time-dependent solution for a δ function pulse of current. The potential is described by a Gaussian function centered at the site of current injection that broadens and shrinks in amplitude over time.

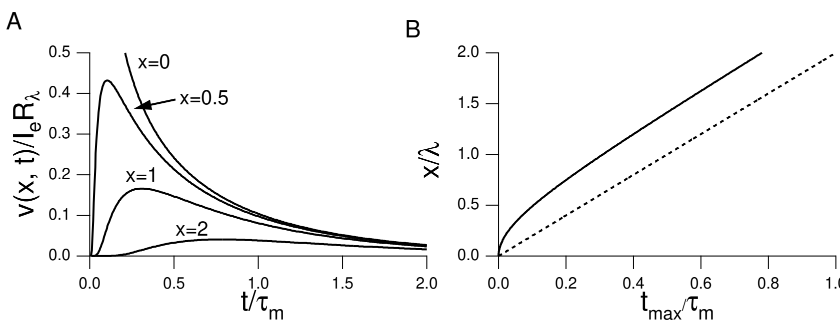

Figure 5.9: Time-dependence of the potential on an infinite cable in response to a pulse of current injected at the point $x = 0$. A) The potential is always largest at the site of current injection. At any fixed point, it reaches its maximum value as a function of time later for measurement sites located further away from the current source. B) Movement of the temporal maximum of the potential. The solid line shows the relationship between the measurement location x, and the time t_{max} when the potential reaches its maximum value at that location. The dashed line corresponds to a constant velocity $2\lambda/\tau_m$.

An Isolated Branching Node

To illustrate the effects of branching on the membrane potential in response to a point source of current injection, we consider a single isolated junction of three semi-infinite cables as shown in figure 5.7A. For simplicity, we discuss the solution for static current injection at a point, but the results generalize directly to the case of time-dependent currents. The solution for the three segments shown in figure 5.7A is (for a derivation see

Abbott, 1992)

$$
\begin{aligned}
v_1(x_1) &= p_1 I_e R_{\lambda_1} \exp(-x_1/\lambda_1 - y/\lambda_2) \\
v_2(x_2) &= \frac{I_e R_{\lambda_2}}{2} \left[\exp(-|y - x_2|/\lambda_2) + (2p_2 - 1)\exp(-(y + x_2)/\lambda_2)\right] \\
v_3(x_3) &= p_3 I_e R_{\lambda_3} \exp(-x_3/\lambda_3 - y/\lambda_2)\,,
\end{aligned}
\tag{5.17}
$$

where, for $i = 1$, 2, and 3,

$$
p_i = \frac{a_i^{3/2}}{a_1^{3/2} + a_2^{3/2} + a_3^{3/2}} \quad , \quad \lambda_i = \sqrt{\frac{r_m a_i}{2r_L}} \quad \text{, and} \quad R_{\lambda_i} = \frac{r_L \lambda_i}{\pi a_i^2}\,. \tag{5.18}
$$

Note that the distances x and y appearing in the exponential functions are divided by the electronic length of the segment along which the potential is measured or the current is injected, respectively. This solution satisfies the cable equation, because it is constructed by combining solutions of the form 5.14. The only term that has a discontinuous first derivative within the range being considered is the first term in the expression for v_2, and this solves the cable equation at the current injection site because it is identical to 5.14. We leave it to the reader (exercise 2) to verify that this solution satisfies the boundary conditions $v_1(0) = v_2(0) = v_3(0)$ and 5.7. The solution for a branching node can also be used to analyze a junction along a cable where the radius suddenly steps up or down. In this case, a_1 and a_2 are the two radii being joined and a_3 is set to zero.

Figure 5.10 shows v_1, v_2, and v_3 at locations $x_1 = \lambda_1$, $x_2 = \lambda_2$, and $x_3 = \lambda_3$ for different locations of the injection site on segment 2. Along segment 2, we see exponential attenuation as the injection site moves away from the recording site. At locations that are one electronic length constant away from junction point, the potentials on segments 1 and 3 are identical. Note that this does not correspond to measuring these potentials at equal distances from the injection point because the electrotonic length constants of segments 1 and 3 are not equal. There is much more attenuation of the potential on segments 1 and 3 when segment 1 is larger than segments 2 and 3 (figure 5.10A), than when it is smaller (figure 5.10B). Dendritic radii tend to get smaller further away from the soma, so that large attenuation in figure 5.10A corresponds to currents injected distally and voltages measured nearer to the soma, while the smaller attenuation in figure 5.10B corresponds to proximal current injection and a more distal voltage measurement.

The expression for v_1 given above (and also that for v_3) has exactly the same form as the solution 5.14 for an infinite cable except for two modifications. The argument of the exponential in equation 5.14, which is the distance between the injection site and the measurement site in units of electrotonic length, is corrected for the fact that segments 1 and 2 have different radii. In addition, the factor of $1/2$ in equation 5.14 is replaced by p_1. The amplitude of the potential, relative to that of an unbranched cable, is either enhanced or decreased depending on whether p_1 is greater than

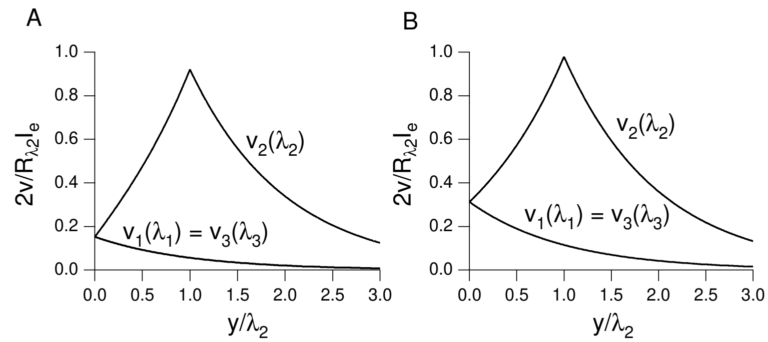

Figure 5.10: The potentials along the three segments of an isolated junction at locations that are one electrotonic length constant away from the junction along each segment. The potentials are plotted as a function of the distance y to the injection site on segment 2, measured in unit of the electrotonic length constant λ_2. The scale for the potentials is in units of $R_{\lambda_2} I_e$. In both cases, the radii of segments 2 and 3 are equal. A) Segment 1 has twice the radius of segments 2 and 3. B) Segment 1 has half the radius of segments 2 and 3.

or less than 1/2. This, in turn, depends on whether $a_1^{3/2}$ is greater than or less than $a_2^{3/2} + a_3^{3/2}$. If $a_1^{3/2} = a_2^{3/2} + a_3^{3/2}$, $p_1 = 1/2$ and the amplitude factor is identical to that for an infinite cable with no junction. This relationship arises in the discussion of the equivalent cable introduced by Rall (1959, 1977) (see below).

The Rall Model

The infinite and semi-infinite cables we have considered are clearly mathematical idealizations. We now turn to a model neuron introduced by Rall (1959, 1977) that, while still highly simplified, contains some important elements that affect the responses of real neurons. Most neurons receive their synaptic inputs over complex dendritic trees that branch out from their somata. The integrated effect of these inputs is usually measured from within the soma, and the spike-initiation region of the axon that determines whether the neuron fires an action potential is typically located near the soma. In Rall's model, a compact soma region (represented by one compartment) is connected to a single equivalent cylindrical cable that replaces the entire dendritic region of the neuron (see the schematics in figures 5.11 and 5.13). More complex models can be constructed along these lines by connecting the soma to multiple equivalent cables, each of which approximates a portion of the full dendritic structure. The critical feature of the model is the choice of radii and lengths for these equivalent cables that best match the properties of the dendritic structures being approximated.

The radius a and length L of the equivalent cable are determined by matching two important elements of the full dendritic tree. These are the total length in electrotonic units, which determines the amount of attenuation, and the total surface area, which determines the total membrane resistance and capacitance. The length of a dendrite in electrotonic units is the sum of lengths measured along a direct path from the soma to the terminals of the dendrite. Along each segment comprising such a path, the length in electrotonic units is the actual length divided by the electrotonic length constant for that segment. In general, the total length measured in this way depends on which terminal of the tree is used as an end point, but an average value can be used for the full dendritic structure. The length L of the dendritic cable is then chosen so that L/λ is equal to this average electrotonic length, where λ is the length constant for the equivalent cable. The radius of the equivalent cable, which is needed to compute λ, is determined by setting the surface area of the equivalent cable, $2\pi aL$ equal to the surface area of the full dendritic tree.

Under some restrictive circumstances the equivalent cable reproduces the effects of a full tree exactly (Rall, 1959 & 1977). Among these conditions is the requirement that the relation $a_1^{3/2} = a_2^{3/2} + a_3^{3/2}$ discussed above must be satisfied at all of the branching nodes of the tree. However, even when it is not exact, the equivalent cable is an extremely useful and often fairly accurate simplification.

Figures 5.11 and 5.13 depict static solutions of the Rall model for two different recording configurations expressed in the form of equivalent circuits. The equivalent circuits are an intuitive way of expressing the solution to the cable equation. In figure 5.11, constant current is injected into the soma. The circuit diagram shows an arrangement of resistors that duplicates the effects of the full model for the purposes of voltage measurements at the soma, v_{soma}, and a distance x along the equivalent cable, $v(x)$. R_{soma} is the membrane resistance of the soma, and

$$R_1 = \frac{R_\lambda \left[\cosh\left(L/\lambda\right) - \cosh\left((L-x)/\lambda\right)\right]}{\sinh\left(L/\lambda\right)} \tag{5.19}$$

$$R_2 = \frac{R_\lambda \cosh\left((L-x)/\lambda\right)}{\sinh\left(L/\lambda\right)} . \tag{5.20}$$

The values for these resistance (and similarly the values of R_3 and R_4 given below) are set so that the equivalent circuit reconstructs the solution of the cable equation obtained using standard methods (see for example Tuckwell, 1988). Expressions for v_{soma} and $v(x)$, arising directly from the equivalent circuit using standard rules of circuit analysis (current conservation and Ohm's law), are given at the right side of figure 5.11.

The input resistance of the Rall model neuron, as measured from the soma, is determined by the somatic resistance R_{soma} acting in parallel with the effective resistance of the cable and is $(R_1 + R_2)R_{\text{soma}}/(R_1 + R_2 + R_{\text{soma}})$. The effective resistance of the cable, $R_1 + R_2 = R_\lambda / tanh(L)$, approaches the

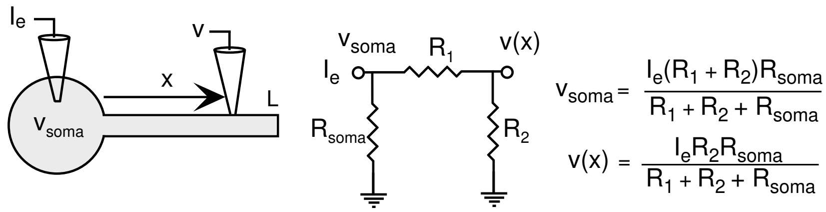

Figure 5.11: The Rall model with static current injected into the soma. The schematic at left shows the recording set up. The potential is measured at the soma and at a distance x along the equivalent cable. The central diagram is the equivalent circuit for this case, and the corresponding formulas for the somatic and dendritic voltages are given at the right. The symbols at the bottom of the resistances R_{soma} and R_2 indicate that these points are held at zero potential. R_{soma} is the membrane resistance of the soma, and R_1 and R_2 are the resistances given in equations 5.19 and 5.20.

value R_λ when $L \gg \lambda$. As we noted previously, the effect of lengthening a cable saturates when it gets much longer than its electrotonic length. The voltage attenuation caused by the cable is defined as the ratio of the dendritic to somatic potentials, and it is given in this case by

$$\frac{v(x)}{v_{\text{soma}}} = \frac{R_2}{R_1 + R_2} = \frac{\cosh\left((L-x)/\lambda\right)}{\cosh\left(L/\lambda\right)} . \tag{5.21}$$

This result is plotted in figure 5.12.

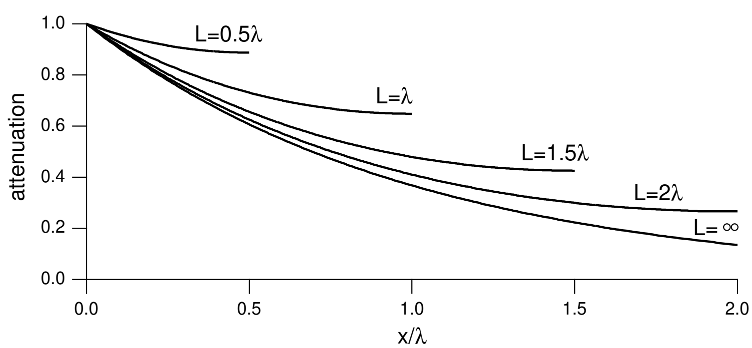

Figure 5.12: Voltage and current attenuation for the Rall model. The attenuation plotted is the ratio of the dendritic to somatic voltages for the recording setup of figure 5.11, or the ratio of the somatic current to the injected current for the arrangement in figure 5.13. Attenuation is plotted as a function of x/λ for different equivalent cable lengths.

Figure 5.13 shows a similar equivalent circuit for the Rall model when current is injected at a location x along the dendritic tree and the soma is clamped at $v_{\text{soma}} = 0$. The equivalent circuit can be used to determine the current entering the soma and the voltage at the site of current injection,

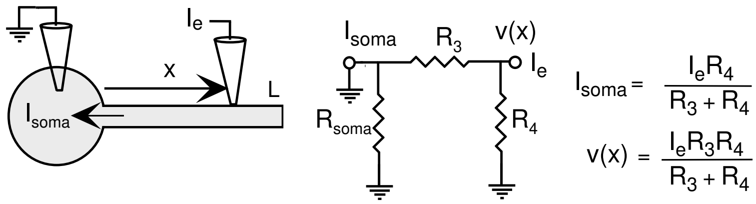

Figure 5.13: The Rall model with static current injected a distance x along the equivalent cable while the soma is clamped at zero potential. The schematic at left shows the recording set up. The potential at the site of the current injection and the current entering the soma are measured. The central diagram is the equivalent circuit for this case, and the corresponding formulas for the somatic current and dendritic voltage are given at the right. R_{soma} is the membrane resistance of the soma, and R_3 and R_4 are the resistances given in equations 5.22 and 5.23.

and the resulting equations are given in the figure. In this case, the somatic resistance is irrelevant because the soma is clamped at zero potential. The other resistances are

$$R_3 = R_\lambda \sinh(x/\lambda) \tag{5.22}$$

and

$$R_4 = \frac{R_\lambda \sinh(x/\lambda)\cosh((L-x)/\lambda)}{\cosh(L/\lambda) - \cosh((L-x)/\lambda)} . \tag{5.23}$$

The input resistance for this configuration, as measured from the dendrite, is determined by R_3 and R_4 acting in parallel and is $R_3 R_4/(R_3 + R_4) = R_\lambda \sinh(x/\lambda)\cosh((L-x)/\lambda)/\cosh(L/\lambda)$. When L and x are both much larger than λ, this approaches the limiting value R_λ. The current attenuation is defined as the ratio of the somatic to injected currents and is given by

$$\frac{I_{\text{soma}}}{I_e} = \frac{R_4}{R_3 + R_4} = \frac{\cosh((L-x)/\lambda)}{\cosh(L/\lambda)} . \tag{5.24}$$

The inward current attenuation (plotted in figure 5.12) for the recording configuration of figure 5.13 is identical to the outward voltage attenuation for figure 5.11 given by equation 5.21. Equality of the voltage attenuation measured in one direction and the current attenuation measured in the opposite direction is a general feature of linear cable theory.

The Morphoelectrotonic Transform

The membrane potential for a neuron of complex morphology is obviously much more difficult to compute than the simple cases we have considered. Fortunately, efficient numerical schemes (discussed in chapter 6) exist for generating solutions in these cases. However, even when the solution is known, it is still difficult to visualize the effects of a complex morphology on the potential. Zador, Agmon-Snir, and Segev (1995) have devised a clever scheme for depicting the attenuation and delay of the membrane potential for complex morphologies. The voltage attenuation, as plotted in figure 5.12, is not an appropriate quantity to represent geometrically because it is not additive. Consider three points along a cable satisfying $x_1 > x_2 > x_3$. The attenuation between x_1 and x_3, in this case, is the product of the attenuation from x_1 to x_2 and from x_2 to x_3, $v(x_1)/v(x_3) = [v(x_1)/v(x_2)][v(x_2)/v(x_3)]$. An additive quantity can be obtained by taking the logarithm of the attenuation, since $\ln(v(x_1)/v(x_3)) = \ln(v(x_1)/v(x_2)) + \ln(v(x_2)/v(x_3))$. The morphoelectrotonic transform is a diagram of a neuron in which the distance between any two points is determined by the logarithm of the ratio of the membrane potential at these two locations, not by the actual size of the neuron.

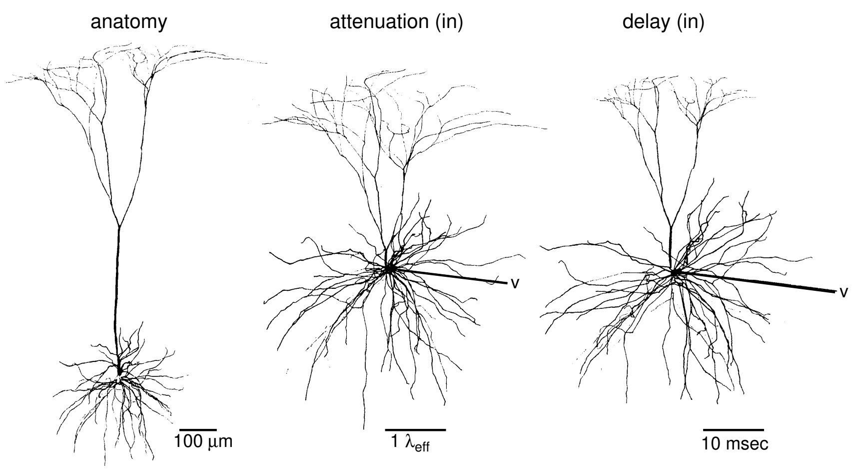

Figure 5.14: The morphoelectrotonic transform of a cortical neuron. The left panel is a normal drawing of the neuron. The central panel is a diagram in which the distance between any point and the soma is proportional to the logarithm of the steady-state attenuation between the soma and that point for static current injected at the terminals of the dendrites. The scale bar denotes the distance corresponding to an attenuation of $\exp(-1)$. In the right panel, the distance from the soma to a given point is proportional to the inward delay, which is the centroid of the soma potential minus the centroid at the periphery when a pulse of current is injected peripherally. The arrows in the diagrams indicate that the reference potential in these cases is the somatic potential. (From Zador et al, 1995)

Another morphoelectrotonic transform can be used to indicate the amount of delay in the voltage waveform produced by a transient input current. The morphoelectrotonic transform uses a different definition of delay than that used in Figure 5.9B. The delay between any two points is defined as the difference between the centroid, or center of 'gravity', of the voltage response at these points. Specifically, the centroid at point x is defined as $\int dt\, t v(x,t) / \int dt\, v(x,t)$. Like the log-attenuation, the delay between any two points on a neuron is represented in the morphoelectrotonic transform as a distance.

Morphoelectrotonic transforms of a pyramidal cell from layer 5 of cat visual cortex are shown in figures 5.14 and 5.15. The left panel of figure 5.14 is a normal drawing of the neuron being studied, the middle panel shows the steady-state attenuation, and the right panel shows the delay. These figures indicate that, for inward moving signals, the apical and basal dendrites are much more uniform than the morphology would suggest. These diagrams correspond to current being injected peripherally, with somatic potentials being compared to dendritic potentials.

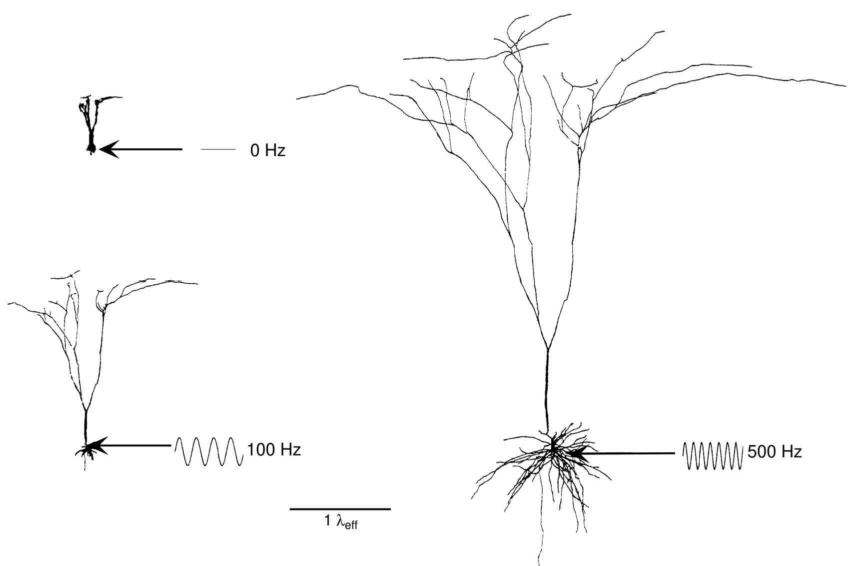

Figure 5.15: Morphoelectrotonic transforms of the same neuron as in figure 5.14 but showing the outward log-attenuation for DC and oscillating input currents. Distances in these diagrams are proportional to the logarithm of the amplitude of the voltage oscillations at a given point divided by the amplitude of the oscillations at the soma when a sinusoidal current is injected into the soma. The upper left panel corresponds to DC current injection, the lower left panel to sinusoidal current injection at a frequency of 100 Hz, and the right panel to an injection frequency of 500 Hz. The scale bar denotes the distance corresponding to an attenuation of $\exp(-1)$. (From Zador et al, 1995)

The small neuron diagram at the upper left of figure 5.15 shows attenuation for the reverse situation from figure 5.14, when DC current is injected into the steady-state soma and dendritic potentials are compared with the somatic potential. Note how much smaller this diagram is than the one in the central panel of figure 5.14. Outward moving signals are attenuated much less than inward moving signals. This is because the soma provides a much larger current sink for signals coming from the thin dendrites than the dendrites provide for signals emerging from the soma. In addition, the morphoelectrotonic diagrams showing attenuation and delay in the outward direction are more similar to the actual morphology of the neuron.

The capacitance of neuronal cables causes the voltage attenuation for time-dependent current injection to increase as a function of frequency. Figure 5.15 compares the attenuation of dendritic potentials relative to the somatic potential when DC or sinusoidal current of two different frequencies is injected into the soma. Clearly, attenuation increases dramatically as a function of frequency. Thus, a neuron that appears electrotonically compact for static or low frequency current injection may be noncompact when higher frequencies are considered. For example, action potential waveforms, that correspond to frequencies around 1000 Hz, are much more severely attenuated within neurons than slower varying potentials.

5.4 Membrane and Synaptic Conductances

Studying the properties of neuron models with linear membrane conductances reveals some aspects of the relationship between morphology and function, but many of the electrical properties of real neurons, including their ability to fire and propagate action potentials, arise from nonlinearities. Membrane conductances are nonlinear because voltage-dependent ion channels are strongly affected by the potential across the membrane in which they are embedded.

Recordings of the current flowing through single channels indicate that channels fluctuate rapidly between open and closed states in a stochastic manner (figure 5.16). The probability that a channel will be found in an open, ion conducting state at any given time can depend on the membrane potential (for a voltage-dependent channel), on the presence or absence of a neurotransmitter (for a synaptic receptor channel), or on a number of other factors such as the concentration of Ca^{2+} or other messenger molecules inside the cell.

Models of membrane and synaptic conductances must account for the effects of membrane potential, neurotransmitters, and other factors on channel conductances. At the end of this chapter, we discuss stochastic models of individual channels based on state diagrams and transition rates. However, most neuron models use deterministic descriptions of the total conductances arising from many channels. This is justified because of the large number of channels of each type in the membrane of a typical neuron. If large numbers of channels are present and if they act independently of each other (which they do to a good approximation), the fraction of channels open at any given time is equal to the probability of any one channel being in an open state. This follows from the law of large numbers, and it allows us to move freely between single channel probabilistic

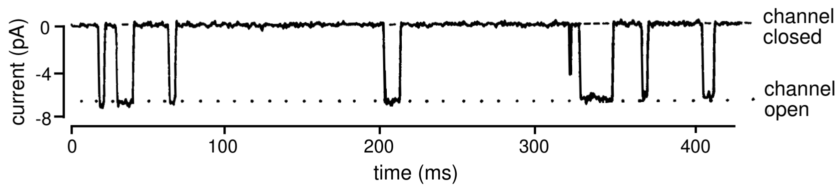

Figure 5.16: Recording of current passing through a single ion channel. This is a synaptic receptor channel sensitive to the neurotransmitter acetylcholine. A small amount of acetylcholine has been applied to the preparation to produce occasional channel openings. In the open state, the channel passes 6.6 pA at a holding potential of -140 mV. This is equivalent to more than 10^7 charges per second passing through the channel and corresponds to an open channel conductance of 47 pS. (From Hille, 1992.)

and macroscopic deterministic descriptions of membrane currents.

Equilibrium and Reversal Potentials

Two forces are responsible for driving ions through channel pores. Any potential difference between the exterior and interior of the cell will produce an electric field and a force on the ions. When a neuron is at rest, its negative potential attracts positive ions into the neuron and repels negative ions. In addition, ions diffuse through channels because the ion concentrations differ inside and outside the neuron. These differences are maintained by ion pumps within the cell membrane. The concentrations of Na^+ and Ca^{2+} are higher outside the cell than inside, so these ions are driven into the neuron by diffusion. K^+ is more concentrated inside the neuron than outside, so it tends to diffuse out of the cell. Cl^- has more equal concentrations in the intra- and extracellular media.

It is convenient to characterize the current flow due to diffusion in terms of an equilibrium potential. This is defined as the membrane potential at which current flow due to electric forces cancels the diffusive flow. For channels that conduct a single type of ion, the equilibrium potential can be computed easily. The potential difference across the cell membrane biases the flow of ions into or out of a neuron. Consider, for example, a positively charged ion and a negative membrane potential. In this case, the membrane potential opposes the flow of ions out of the the cell. Ions can only cross the membrane and leave the interior of the cell if they have sufficient thermal energy to overcome the energy barrier produced by the membrane potential. If the ion has an electric charge zq where q is the charge of one proton, it must have a thermal energy of at least $-zqV$ to cross the membrane. The probability that an ion has a thermal energy greater than or equal to $-zqV$, when the temperature (on an absolute scale) is T, is $\exp(zqV/k_BT)$. This is determined by integrating the Boltzmann distribution for energies greater than or equal to $-zqV$. In molar units, this result can be written as $\exp(zFV/RT)$, which is equal to $\exp(zV/V_T)$ by equation 5.1.

The biasing effect of the electrical potential can be overcome by an opposing concentration gradient. If there are more ions inside the neuron than outside it, the effect of the difference in ion concentrations can compensate for the Boltzmann probability factor. The rate at which ions flow into the cell is proportional to the concentration of ions outside the cell, [outside], The flow of ions out of the cell is proportional to the concentration of ions inside the cell, [inside], times the Boltzmann factor, because in this direction only those ions that have sufficient thermal energy can enter the cell. The net flow of ions will be zero when the inward and outward flows are equal. We use the letter E to denote the particular potential that satisfies this balancing condition which is then

$$[\text{outside}] = [\text{inside}]\exp(zE/V_T)\,. \tag{5.25}$$

Solving this equation for E, we find

$$E = \frac{V_T}{z}\ln\left(\frac{[\text{outside}]}{[\text{inside}]}\right)\,. \tag{5.26}$$

Equation 5.26 is the Nernst equation. The reader can check that, if the result is derived for either sign of ionic charge or membrane potential, the result is identical to 5.26 which thus applies in all cases (exercise 5).

The following tables (adapted from Johnston and Wu, 1995) give typical values of ion concentrations and equilibrium potentials for different ions in two preparations.

Squid Axon, $T = 20^\circ$

ion	[inside] (mM)	[outside] (mM)	E (mV)
K^+	400	20	-77
Na^+	50	440	57
Cl^-	52	560	-62
Ca^{2+}	10^{-4}	10	150

Typical Mammalian Neuron, $T = 37^\circ$

ion	[inside] (mM)	[outside] (mM)	E (mV)
K^+	140	5	-89
Na^+	10	145	71
Cl^-	4	110	-61
Ca^{2+}	10^{-4}	4	148

The Nernst equation (5.26) applies when the channels that generate a particular conductance allow only one type of ion to pass through them. Some channels are not so selective, and in this case the equilibrium potential is not determined by equation 5.26, but rather takes a value intermediate between the equilibrium potentials of the individual ion types that it conducts. An approximate formula known as the Goldman equation (see Tuckwell, 1988; or Johnston and Wu, 1995) can be use to estimate E for such conductances.

A conductance with equilibrium potential E tends to move the membrane potential of the neuron toward the value E. When $V > E$ this means that the current will be positive and when $V < E$ it will be negative. For this reason, E is also called the reversal potential. Reversal potential is a more general term for E that can be applied even when the permiabilities of a given conductance to different types of ions are not known. Na^+ and Ca^{2+} conductances have positive reversal potentials so they typically depolarize a neuron (make its membrane potential less negative). K^+ conductances, with their negative E values, normally hyperpolarize a neuron (make its membrane potential more negative). Cl^- conductances have reversal potentials near the resting potential of most neurons, and when the membrane potential is near this value they may pass little net current. Instead, their primary impact is to change the membrane resistance of the cell. Such conductances are sometimes called shunting, although all conductances 'shunt', that is, increase the total conductance of a neuron. Shunting is an important interaction between synaptic inputs that can cause one set of inputs to reduce the efficacy of another set.

Membrane and Synaptic Currents

We denote the conductance per unit area of membrane due to ion channels of type i by g_i, where i labels the channel type. The total conductance is the product of the conductance of an open channel, the density of channels in the membrane, and the fraction of channels that are open at any given time. The product of the first two factors is called the maximal conductance, $\overline{g}_i$, which is the total conductance per unit area of membrane if all the channels of type i are open. Maximal conductances tend to range from μS/mm^2 to mS/mm^2. The fraction of channels in the open state is equal to the probability of finding any given channel in the open state, and it is denoted by P_i. Thus, $g_i = \overline{g}_i P_i$.

To make use of mathematical descriptions of membrane conductances in neuron models, we must know how the membrane or synaptic currents per unit area, i_m or i_s, are related to the conductances g_i. For most conductances, the current flowing through a set of channels is assumed to increase or decrease linearly when the membrane potential deviates from the reversal potential. For many channels, this is a fairly accurate approximation. The difference $V - E_i$ is called the driving force. The membrane current per unit area due to conductance i is thus $g_i(V - E_i)$. By convention, these currents are defined as positive when positive ions leave the neuron. The total membrane current due to a number of conductances is determined simply by summing their individual contributions.

Sometimes a different equation, known as the constant field or Goldman-

Hodgkin-Katz model, is used to describe the total current flowing through a conductance, so the membrane current per unit area is written as

$$\frac{g_i V_T \left(1 - \exp(-zE_i/V_T)\right)}{zE} \left(\frac{V\left(\exp(zV/V_T) - \exp(zE_i/V_T)\right)}{\exp(zV/V_T) - 1} \right) . \qquad (5.27)$$

This equation is based on an analysis of the effects of diffusion and electric fields on the movement of ions within a channel pore. The calculation is based on approximating the electric field within a channel pore as constant (hence the name). For a derivation, see Tuckwell (1988) or Johnston and Wu (1995). Figure 5.17 compares the current given by the above expression with the current of the linear model.

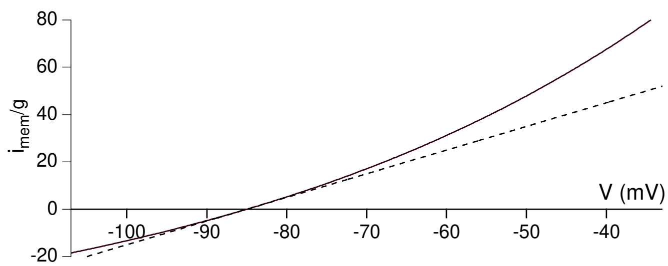

Figure 5.17: Membrane currents of the linear and constant field models as a function of membrane potential. The solid line is the current of the constant field model, equation 5.27, and the dashed curve is the linear expression $i_{mem} = g(V - E)$. The reversal potential in this case is $E = -85$ mV.

The dynamics of a given conductance is determined by the open probability, P_i, which can depend on a large number of factors. The open probability of a voltage-dependent conductance depends, as its name suggests, on the membrane potential of the neuron. In this chapter, we discuss models of two such conductances, the delayed-rectifier K^+ and fast Na^+ conductances. The formalism we present, which is almost universally used to describe voltage-dependent conductances, was developed by Hodgkin and Huxley as part of their pioneering work on these conductances and how they account for action potential generation in the squid giant axon (Hodgkin and Huxley, 1952). Other conductances are modeled in chapter 6. A number of other factors can affect the open probability of a channel in addition to voltage. Of particular importance are calcium-dependent conductances that have open probabilities affected by the intracellular Ca^{2+} concentration. For example, calcium-dependent potassium conductances increase when the intracellular calcium concentration rises.

If a conductance has $P_i = 1$ (or any other constant value) at all times, it is termed passive or linear. All of the conductances that remain at relatively constant values, at least on the time scale of a particular phenomenon being studied, are typically grouped together into a single term called the leakage conductance. Of particular importance in this category are the currents carried by ion pumps. The concentration gradients that make equilibrium potentials nonzero are maintained by ion pumps located in the cell membrane. For example, one type of pump uses the energy of ATP hydrolysis to move three Na^+ ions out of the cell for every two K^+ ions it moves in. It is normally assumed that these pumps work at relatively steady rates so that the currents they generate can be included in a time-independent leakage conductance. Sometimes, this assumption is dropped and explicit pump currents are modeled. In either case, all of the time-independent contributions to the membrane current are lumped together into a single leakage term $\overline{g}_L(V - E_L)$. Because this term hides many sins, its reversal potential E_L is not usually equal to the equilibrium potential of any specific ion. Instead it is often kept as a free parameter and adjusted to make the resting potential of the model neuron match that of the cell being modeled. Similarly, $\overline{g}_L$ is adjusted to match the membrane conductance at rest.

Synaptic conductances are distinguished by having open probabilities that depend on the presence of a neurotransmitter. Like membrane currents, synaptic currents are expressed as the product of a synaptic conductance times a driving force $g_s(V - E_s)$. The synaptic conductance can be written as a maximal conductance times an open probability, $g_s = \overline{g}_s P_s$. Synapses with synaptic reversal potentials E_s greater than the resting potential of the neuron are called excitatory while those with E_s less than the resting potential are called inhibitory. Synapses with reversal potentials near the resting potential are termed shunting and, like all synaptic conductances with reversal potentials below the threshold for action potential generation, are considered inhibitory.

Voltage-Dependent Membrane Conductances

Figure 5.18 shows cartoons of the mechanisms by which voltage-dependent channels open and close as a function of membrane potential. Figures 5.18A and 5.18B depict channels for two different types of conductances termed persistent (5.18A) and transient (5.18B). We begin by discussing persistent conductances.

Persistent Conductances

Figure 5.18A shows a swinging gate attached to a voltage sensor that can open or close the pore of the channel. In reality, channel gating mechanisms involve complex changes in the conformational structure of the channel, but the simple swinging gate picture is sufficient if we are only interested in the current carrying capacity of the channel. A channel that acts as if it had a single gate, like the channel in figure 5.18A produces what is called a persistent or noninactivating conductance. Opening of the gate is called activation of the conductance and gate closing is called

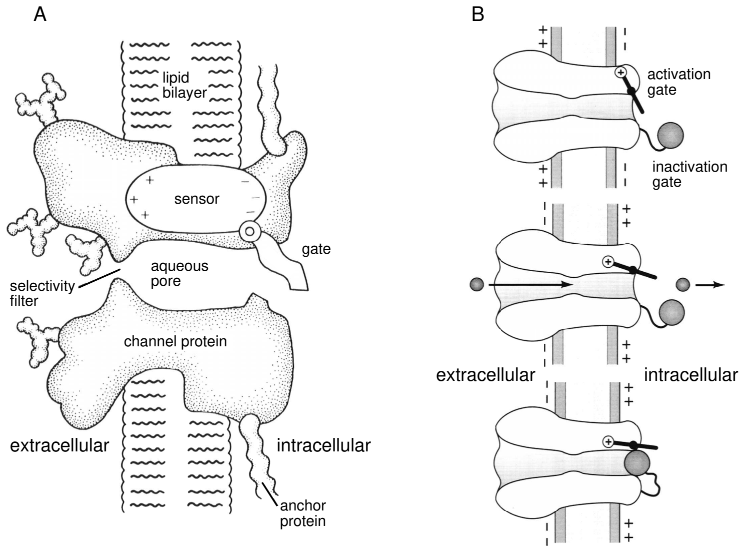

Figure 5.18: Gating of membrane channels. In both figures, the interior of the neuron is to the right of the membrane, and the extracellular medium is to the left. A) A cartoon of gating of a persistent conductance. A single gate is opened and closed by a sensor that responds to the membrane potential. The channel also has a region that selectively allows ions of a particular type to pass through the channel, for example, K^+ ions for a potassium channel. B) A cartoon of the gating of a transient conductance. The activation gate is coupled to a voltage sensor (denoted by a circled $+$) and acts like the gate in A. A second gate, denoted by the ball, can block that channel once it is open. The top figure shows the channel in a deactivated (and deinactivated) state. The middle panel shows an activated channel, and the bottom panel shows an inactivated channel. Only the middle panel corresponds to an open, ion-conducting state. (A from Hille, 1992; B from Kandel *et al*, 1991)

deactivation. For this type of channel, P increases when the neuron is depolarized and decreases when it is hyperpolarized. The delayed-rectifier K^+ conductance that is responsible for repolarizing a neuron after an action potential is a persistent conductance.

The opening of the single gate that describes a persistent conductance may involve a number of conformational changes. For example, the delayed-rectifier K^+ conductance is constructed from four identical subunits, and it appears that all four must undergo a structural change for the channel to open. In general, if p independent, identical processes are required for a channel to open, P can be written as

$$P = n^p \tag{5.28}$$

where n is the probability that any one of the p independent sub-processes has occurred (n varies between zero and one). In practice, p is an integer chosen to best fit the data but, in some cases, its value corresponds to what is known about the structure of the channel. For example, Hodgkin and Huxley used $p = 4$ to describe the open probability of the delayed-rectifier K^+ channel, which, although they did not know it at the time, is consistent with the four-subunit structure of the channel.

With the open probability written as n^p, the description of the conductance comes down to accounting for the voltage and time dependence of n. It is convenient to think of the process described by n as the opening of a subunit, but this description should not be taken too literally. The equations below account for the macroscopic current through a set of channels, but they are not based on a microscopic description of channel structure. We describe the transition of each subunit by a simple kinetic scheme in which the transition close $\rightarrow$ open occurs at a voltage-dependent rate $\alpha_n(V)$, and the reverse transition open $\rightarrow$ closed occurs at a voltage-dependent rate $\beta_n(V)$. The probability per unit time that a subunit opens is the probability of finding the subunit closed, $1 - n$, times the opening rate $\alpha_n(V)$. Likewise, the probability per unit time that a subunit closes is the probability of finding the subunit open, n, times the closing rate $\beta_n(V)$. The rate at which the open probability for a subunit changes is given by the difference of these two terms

$$\frac{dn}{dt} = \alpha_n(V)(1-n) - \beta_n(V)n. \tag{5.29}$$

The first term describes the opening process and the second term the closing process (hence the minus sign since this lowers the probability of being in the open configuration). This is the basic equation for modeling all macroscopic conductances.

Equation 5.29 can be written in another useful form by dividing through by $\alpha_n(V) + \beta_n(V)$ to obtain

$$\tau_n(V)\frac{dn}{dt} = n_\infty(V) - n \tag{5.30}$$

where

$$\tau_n(V) = \frac{1}{\alpha_n(V) + \beta_n(V)} \tag{5.31}$$

and

$$n_\infty(V) = \frac{\alpha_n(V)}{\alpha_n(V) + \beta_n(V)}. \tag{5.32}$$

Equation 5.30 indicates that for a fixed voltage V, n approaches the limiting value $n_\infty(V)$ exponentially with time constant $\tau_n(V)$.

The key elements in the equation that determines n are the opening and closing rate functions $\alpha_n(V)$ and $\beta_n(V)$, and these must be obtained from experimental measurements. Nevertheless, it is useful to derive the form that we might expect these rate functions to take on the basis of thermodynamic arguments. The state transitions described by α_n and β_n are likely to be rate-limited by barriers requiring thermal energy. These transitions involve the movement of charges across the membrane so the height of these energy barriers should depend on the membrane potential. We expect a given barrier energy to be the sum of a term that is independent of V, reflecting conformational changes that do not move charges across the membrane, and a term that is proportional to qV reflecting the movement of charges across the membrane. We therefore write the barrier energy for the opening transition of a subunit as $qB_\alpha(V - V_\alpha)$ where B_α and V_α are constants. The probability that thermal fluctuations will provide enough energy to surmount this energy barrier is proportional to the Boltzmann factor, the exponential of the negative of the amount of energy needed divided by $k_B T$. Based on this argument, we expect α_n, expressed in units of 1/ms, to be of the form

$$\alpha_n(V) = \exp(-qB_\alpha(V - V_\alpha)/k_B T) = \exp(-B_\alpha(V - V_\alpha)/V_T)\,. \tag{5.33}$$

The closing rate β_n should be expressed similarly except with different constants B_β and V_β. From equation 5.32, we then find that $n_\infty(V)$ is expected to be a sigmoidal function

$$n_\infty(V) = \frac{1}{1 + \exp(-A_n(V - V_n))} \tag{5.34}$$

with $A_n = (B_\beta - B_\alpha)/V_T$ and $V_n = (B_\beta V_\beta - B_\alpha V_\alpha)/(B_\beta - B_\alpha)$. Similarly, in ms units,

$$\tau_n(V) = \frac{1}{\exp(-B_\alpha(V - V_\alpha)/V_T) + \exp(-B_\beta(V - V_\beta)/V_T)}\,. \tag{5.35}$$

For a voltage-activated conductance, depolarization causes n and P to grow toward one, and hyperpolarization causes them to shrink toward zero. Thus, we expect that the opening rate, α_n should be an increasing function of V (and thus $B_\alpha < 0$) and β_n should be a decreasing function of V (and thus $B_\beta > 0$). Examples of the functions we have discussed are plotted in figure 5.19.

While thermodynamic arguments support the forms we have presented, they rely on simplistic assumptions. Not surprisingly, the resulting functional forms do not always fit the data and various alternatives are often used. Hodgkin and Huxley used the exponential form we have discussed (with $V_\beta = 231$ mV and $B_\alpha/V_T = 0.0125$/mV, see figure 5.19) to fit the closing rate function $\beta_n(V)$ for the delayed-rectifier K^+ conductance they studied in the squid giant axon. However, they used a different formula for $\alpha_n(V)$,

$$\alpha_n = \frac{.01(V + 55)}{1 - \exp[-.1(V + 55)]}\,, \tag{5.36}$$

where V is expressed in mV, and α_n is in units of 1/ms. The dashed curves in figure 5.19 are the actual fits of Hodgkin and Huxley. The two fits agree quite well. The modifications introduced by Hodgkin and Huxley to match their data are much more significant for fits of the Na^+ conductance.

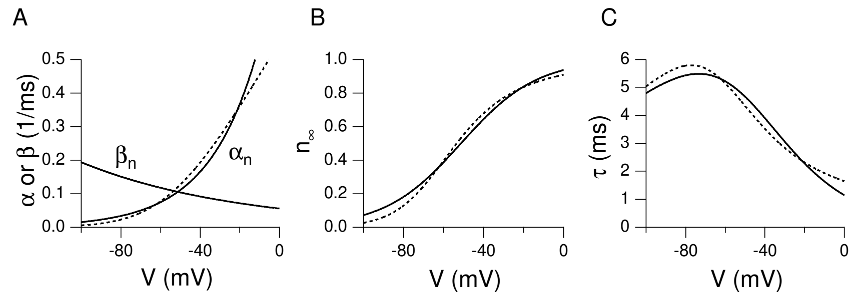

Figure 5.19: Generic voltage-dependent gating functions compared with Hodgkin-Huxley results for the delayed-rectifier K^+ conductance. A) The exponential α_n and β_n functions expected from thermodynamic arguments are indicated by the solid curves. Parameter values used were $V_\alpha = -5$ mV, $V_\beta = -231$ mV, $B_\alpha / V_T = -0.04$/mV, and $B_\beta / V_T = 0.0125$/mV. The fit of Hodgkin and Huxley for β_n is identical to the solid curve shown. The Hodgkin-Huxley fit for α_n is the dashed curve. B) The resulting function $n_\infty(V)$ of equation 5.34 (solid curve). The dashed curve is obtained using the α_n and β_n functions of the Hodgkin-Huxley fit. C) The resulting function $\tau_n(V)$ of equation 5.35 (solid curve). Again the dashed curve is the result of using the Hodgkin-Huxley rate functions.

Transient Conductances

Figure 5.18B is a schematic of a channel controlled by two gates that generates a transient conductance. The swinging gate in figure 5.18B behaves exactly like the gate in figure 5.18A. The probability that it is open is written as m^p where m is a variable similar to n called the activation variable. The ball in figure 5.18B acts as a second gate and the probability that the ball does not block the channel pore is written as h^q where h is called the inactivation variable. The integer powers p and q allow for opening and closing transitions that involve multiple process as discussed above. In their model of the fast Na^+ conductance, Hodgkin and Huxley used $p = 3$ and $q = 1$. For the channel in figure 5.18B to conduct, both gates must be open, and, assuming the two gates act independently, this has probability

$$P = m^p h^q \,, \tag{5.37}$$

This is the general form used to describe the open probability for a transient conductance. The activation m and inactivation h, which are also called gating variables, vary between zero and one. They are described by equations identical to 5.29, except that the variable and subscripts n are replaced by m and h, and the α and β functions are given by (in units of 1/ms with V in mV)

$$\alpha_m = \frac{.1(V+40)}{1-\exp[-.1(V+40)]} \qquad \beta_m = 4\exp[-.0556(V+65)]$$
$$\alpha_h = .07\exp[-.05(V+65)] \quad \beta_h = 1/(1+\exp[-.1(V+35)]) \,. \tag{5.38}$$

A conductance of this type is transient because the activation and inactivation variables m and h have opposite voltage dependences. This is what distinguishes the activation and inactivation processes. Depolarization causes m to increase and h to decrease, and hyperpolarization decreases m while increasing h. The same thermodynamic arguments given above for α_n and β_n can be used to deduce exponential forms for the rate factors α_m and β_m. The inactivation rates α_h and β_h are also expected to have exponential forms, but with the opposite voltage dependence; α_h is a decreasing and β_h an increasing function of V. Equation 5.38 shows that β_m and α_h have the expected exponential form, while α_m has the same form used to fit α_n. On the other hand, the function β_h has a sigmoidal shape quite unlike the expected exponential form. We will discuss this discrepancy when we model the Na^+ channel in a later section. Functions $m_\infty(V)$ and $h_\infty(V)$ describing the steady-state activation and inactivation levels, and voltage-dependent time constants for m and h can be defined as in equations 5.32 and 5.31. These are plotted in figure 5.20. For comparison, $n_\infty(V)$ and $\tau_n(V)$ for the K^+ conductance are also plotted. Note that $h_\infty(V)$ is flipped relative to $m_\infty(V)$ and $n_\infty(V)$, so that it approaches one at hyperpolarized voltages and zero at depolarized voltages.

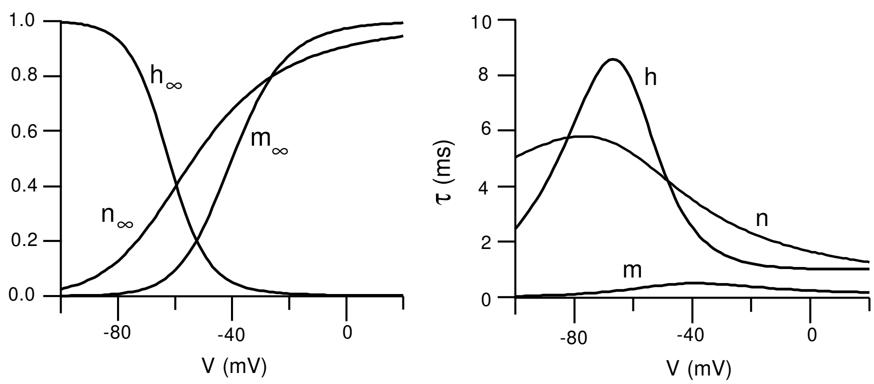

Figure 5.20: The voltage-dependent functions of the Hodgkin-Huxley model. The left panel shows $m_\infty(V)$, $h_\infty(V)$, and $n_\infty(V)$, the steady-state levels of activation and inactivation of the Na^+ conductance and activation of the K^+ conductance. The right panel shows the voltage-dependent time constants that control the rates at which these steady-state levels are approached for the three gating variables.

The presence of two factors in equation (5.37) gives a transient conductance some interesting properties. In order to turn on an inactivating conductance, it may be necessary to first hyperpolarize the neuron and then to depolarize it. Hyperpolarizing the membrane raises the value of the inactivation h, a process called deinactivation. The second step, depolarization, increases the value of the activation m, a process known as activation. Only when m and h are both nonzero is the conductance turned on. Note that the conductance can be reduced in magnitude either by decreasing m or h. Decreasing m is called deactivation to distinguish it from decreasing h which is called inactivation.

Hyperpolarization-Activated Conductances

Persistent currents act as if they are controlled by an activation gate and transient currents by both an activation and an inactivation gate. Another class of conductances, the hyperpolarization-activated conductances, behave as if they are controlled solely by an inactivation gate. They are thus persistent conductances, but they open when the neuron is hyperpolarized because this is what opens an inactivation gate. The opening probability for such channels can be written as $P_i = h^q$, with h described as it is for a transient conductance. Strictly speaking these conductances deinactivate when they turn on and inactivate when they turn off. However, most people cannot bring themselves to say deinactivate all the time, so they say instead that these conductances are activated by hyperpolarization.

The Hodgkin-Huxley Model

The Hodgkin-Huxley model is a description of action potential generation based on the K^+ and Na^+ conductances we have discussed. Simulation of a small portion or an entire length of axon using this model is discussed in chapter 6. Nevertheless, it is instructive to show the results of such a simulation here to illustrate the behavior of the m, h, and n variables during an action potential. The upper trace in figure 5.21 shows the membrane potential for a small segment of axon simulated using the Hodgkin-Huxley model. The other traces indicate how the total membrane current and the m, h, and n variables vary during the course of the action potential.

The initial rise of the membrane potential, prior to the action potential, in figure 5.21 is due to the injection of a positive current into the model axon. When this current drives the membrane potential up to about about -50 mV the m variable that describes activation of the Na^+ conductance suddenly jumps from nearly zero to a value near one. The rapid increase in both V and m is due to a positive feedback effect. Depolarization of the membrane potential causes m to increase, and the resulting activation of the Na^+ conductance causes V to increase. Soon after the rapid depolarization, the h variable, expressing the degree of inactivation of the Na^+ conductance, is around 0.6. Thus, for a brief period both m and h are significantly different from zero. This causes are large influx of Na^+ ions producing the sharp downward spike of inward current shown in the second trace from the top. The inward current pulse causes the membrane potential to rise suddenly to around 50 mV (near the Na^+ equilibrium potential). The rise in the membrane potential causes the Na^+ conductance to inactivate by driving h toward zero. In addition, it activates the K^+ conductance by driving n toward one. This shuts off the Na^+ current and increases the K^+ current so that the total current becomes outward, driving the membrane potential back toward its initial value. The final recovery involves the re-adjustment of m, h, and n back to their initial values.

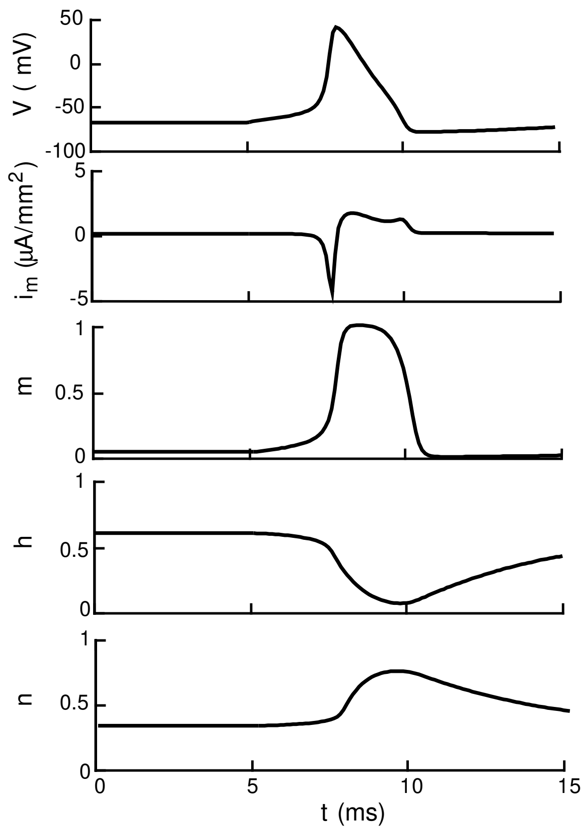

Figure 5.21: The dynamics of m, h, and n in the Hodgkin-Huxley model during the firing of an action potential. The upper trace is the membrane potential, the second trace is the membrane current produced by the sum of the Hodgkin-Huxley K^+ and Na^+ conductances, and subsequent traces show the temporal evolution of m, h, and n.

A Sampling of Membrane Conductances

The electrical properties of neurons arise from the expression of a large number of membrane conductances with a wide variety of properties. Anything more than a superficial listing of these conductances is beyond the scope of this book (see Hille, 1992 or Johnston and Wu, 1995), but even an abbreviated list is useful.

In addition to the fast Na^+ conductance described above, which is responsible for generating action potentials, many neurons have a persistent or very slowly inactivating Na^+ conductance that can maintain membrane potential depolarizations to support sustained firing of action potentials. A number of different Ca^{2+} conductances are commonly found. These are categorized as L, T, N, and P types. L-type Ca^{2+} currents are persistent as far as their voltage dependence is concerned, and they activate at a relatively high threshold. They inactivate due to a Ca^{2+}-dependent rather than voltage-dependent process. T-type Ca^{2+} currents have lower activation thresholds and are transient. They act like slower versions of the fast Na^+ conductance and can generate sustained pulses of depolarization called Ca^{2+} spikes. The depolarization during a Ca^{2+} spike typically generates a burst of action potentials. N- and P-type Ca^{2+} conductances have intermediate thresholds and are respectively transient and persistent. They may be responsible for the Ca^{2+} entry that causes the release of transmitter at presynaptic terminals.

K^+ conductances come in more varieties than any other type. The repolarization of the membrane potential after an action potential is often carried out both by the delayed-rectifier K^+ conductance we have described, and by a fast Ca^{2+}-dependent K^+ conductance. A slower Ca^{2+}-dependent K^+ conductance called the after-hyperpolarization (AHP) current builds up during a sequence of action potentials, gradually slowing the firing rate of the neuron, a process called spike-rate adaptation (see chapter 6). The M-current, another K^+ conductance, also contributes to spike-rate adaptation. It can be blocked by activation of muscarinic acetylcholine receptors, thereby allowing spike-rate adaptation to be modulated. Finally, a transient K^+ conductance, the A-current, helps a neuron to fire at a low rate (see chapter 6) and introduces delays in the firing of action potentials after periods of hyperpolarization.

Hyperpolarization-activated conductances can help a neuron avoid large, prolonged hyperpolarizations and can cause a neuron to rebound when it is released from hyperpolarization. This contributes to a phenomenon called postinhibitory rebound in which a neuron is depolarized following the termination of an inhibitory synaptic input. An example of a conductance in this class is the current I_{h}, which is a mixed-cation current activated by hyperpolarization.

Spike-Mediated Synaptic Conductances

Synaptic transmission at a spike-mediated chemical synapse begins when an action potential invades the presynaptic terminal and activates voltage-dependent Ca^{2+} channels leading to a rise in the concentration of Ca^{2+} within the terminal. This causes vesicles containing transmitter molecules to fuse with the cell membrane and release their contents into the synaptic cleft between the pre- and postsynaptic sides of the synapse. The transmitter molecules then diffuse across the synaptic cleft and bind to receptors on the postsynaptic neuron. Binding of transmitter molecules leads to the opening of an ion channel that modifies the conductance of the postsynaptic neuron, completing the transmission of the signal from one neuron to the other. Postsynaptic ion channels can be activated directly by binding to the transmitter, or indirectly when the transmitter binds to a distinct receptor that affects the ion channel through an intracellular second-messenger signaling pathway.

The open probability for a synaptic conductance P_s can be expressed as a product of two terms that reflect processes occurring on the pre- and postsynaptic side of the synapse, $P_s = P_{rel}s$. The factor s is the probability that a given postsynaptic channel opens when transmitter is released. Since there are typically many postsynaptic channels, this is also the fraction of channels opened by the transmitter. P_{rel} is related to the probability that transmitter is released by the presynaptic terminal following the arrival of an action potential. The interpretation of P_{rel} is subtle because a synaptic connection between neurons may involve multiple anatomical synapses, and each of these may involve multiple independent transmitter release sites. The factor P_{rel}, in our discussion, is the average of the release probabilities at each release site. If there are many release sites, the total amount of transmitter released by all the sites is proportional to P_{rel}. If there is a single release site, P_{rel} is the probability that it releases transmitter. We will restrict our discussion to these two interpretations of P_{rel}. For a modest number of release sites with widely varying release probabilities, the current we discuss only describes an average over multiple trials.

The Postsynaptic Conductance

In a simple model of a directly activated receptor channel, the transmitter interacts with the channel through a binding reaction of the form

$$\text{closed receptor} + n \text{ transmitter molecules} \rightleftharpoons \text{open receptor}\,. \tag{5.39}$$

If the concentration of transmitter at the site of the synaptic channel is $[T]$, the probability of finding n transmitter molecules within binding range of the channel is proportional to $[T]^n$. To determine the rate of channel opening we must multiply this by the probability of finding a channel in the closed state, $1 - s$, and by the opening rate constant, which we denote by k_{open}. The rate of channel closing is the probability of finding the channel open, s, times the closing rate constant k_{close}. Note that k_{open} and k_{close} are expressed in different units since both $k_{open}[T]^n$ and k_{close} have units of one over time. Putting these terms together, we find that the rate at which the open probability changes is

$$\frac{ds}{dt} = k_{open}[T]^n(1 - s) - k_{close}s\,. \tag{5.40}$$

The steady-state open probability given by this equation is

$$s_\infty = \frac{k_{open}[T]^n}{k_{close} + k_{open}[T]^n}\,. \tag{5.41}$$

Using this expression and dividing equation (5.40) by $k_{close} + k_{open}[T]^n$, we can write

$$\tau_s(1 - s_\infty)\frac{ds}{dt} = s_\infty - s \tag{5.42}$$

with $\tau_s = 1/k_{\text{close}}$. This equation indicates that s approaches the value s_∞ asymptotically, and that the time scale for this process is $\tau_s(1 - s_\infty)$.

If no transmitter has been released by the presynaptic terminal for some time, $[T]$, s_∞, and s will all be zero. When an action potential invades the presynaptic terminal, the transmitter concentration rises rapidly and s_∞ reaches a value near one. This causes s to rise toward $s_\infty \approx 1$. The time constant for this process is $\tau_s(1 - s_\infty)$, which is typically much smaller than τ_s because s_∞ is close to one. Following the release of transmitter, diffusion out of the cleft, enzyme-mediated degradation, and presynaptic uptake mechanisms can all contribute to rapidly reducing the transmitter concentration. This sets $[T]$ and s_∞ to zero, and s follows suit by decaying exponentially with time constant τ_s. Note that the time constant for channel closing, τ_s, is considerably larger than the time constant for opening.

Figure 5.22 shows a fit of the model described above to recorded postsynaptic currents. In this case, τ_s was set to 5.26 ms, and the transmitter concentration was modeled as a square pulse of duration 1 ms during which $s_\infty = 0.83$. The time constant determining the rapid rise seen in figure 5.22A is thus $5.26(1 - 0.83)$ ms = 0.9 ms, while the fall of the current is an exponential with a time constant of 5.26 ms.

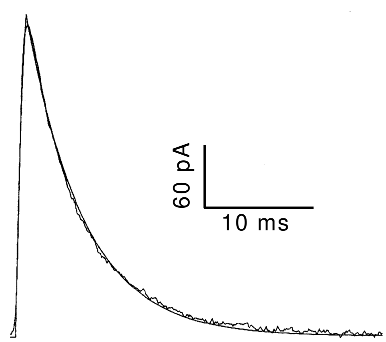

Figure 5.22: A fit of the model discussed in the text to the average EPSC (excitatory postsynaptic current) recorded from mossy fiber input to a CA3 pyramidal cell in a hippocampal slice preparation. The smooth line is the theoretical curve and the wiggly line is the result of averaging recordings from a number of trials. (Adapted from Destexhe *et al*, 1994)

The formalism we have described for computing s requires knowledge of the transmitter concentration, but the exact time course of the transmitter concentration within the synaptic cleft following a presynaptic action potential is not known. As a result, s is often modeled directly without reference to either $[T]$ or s_∞. For a fast synapse like the one shown in figure 5.22, the rise of the conductance following a presynaptic action potential is so rapid that it can be approximated as instantaneous. In this case, the synaptic conductance due to a single presynaptic action potential occurring at $t = 0$ is often written as an exponential, $s = s_{\max} \exp(-t/\tau_s)$

(see the AMPA trace in figure 5.23A). The parameter $s_{\max}$ determines the maximum value of s, and τ_s sets the decay time for the exponential. The synaptic conductance due to a sequence of action potentials at arbitrary times can be modeled by allowing s to decay exponentially to zero according to the equation

$$\tau_s \frac{ds}{dt} = -s\,, \tag{5.43}$$

and incrementing s by $s \rightarrow s + s_{\max}$ immediately after each presynaptic action potential.

If the synapse is not so fast, it may be necessary to model the rise as well as the fall of the synaptic conductance. One way of doing this is to express s as the difference of two exponentials (see the $\mathrm{GABA_A}$, $\mathrm{GABA_B}$, and NMDA traces in figure 5.23). For a presynaptic action potential occurring at $t = 0$, the synaptic conductance is expressed as

$$s = s_{\max}\left(\left(\frac{\tau_2}{\tau_1}\right)^{\tau_{\mathrm{rise}}/\tau_2} - \left(\frac{\tau_2}{\tau_1}\right)^{\tau_{\mathrm{rise}}/\tau_1}\right)^{-1}\big(\exp(-t/\tau_1) - \exp(-t/\tau_2)\big) \tag{5.44}$$

where $\tau_{\mathrm{rise}} = \tau_1\tau_2/(\tau_1 + \tau_2)$ and $\tau_1 > \tau_2$. The rise time of the synapse is determined by τ_{rise} while the fall time is set by τ_1. The rather complicated factor involving the different time constants in equation 5.44 assures that the peak value is equal to the parameter $s_{\max}$. This conductance reaches its peak value a time $\tau_{\mathrm{rise}}\ln(\tau_1/\tau_2)$ after the presynaptic action potential. For sequences of action potentials, this form of synaptic conductance is most easily modeled by expressing s in terms of two auxiliary variables,

$$s = \left(\left(\frac{\tau_2}{\tau_1}\right)^{\tau_{\mathrm{rise}}/\tau_2} - \left(\frac{\tau_2}{\tau_1}\right)^{\tau_{\mathrm{rise}}/\tau_1}\right)^{-1}(s_1 - s_2)\,, \tag{5.45}$$

that satisfy the equations

$$\tau_1 \frac{ds_1}{dt} = -s_1 \quad \text{and} \quad \tau_2 \frac{ds_2}{dt} = -s_2\,. \tag{5.46}$$

Immediately after each presynaptic action potential these variables are incremented by $s_1 \rightarrow s_1 + s_{\max}$ and $s_2 \rightarrow s_2 + s_{\max}$. Note that this produces an s that is initially zero but that rises as s_2 decays faster than s_1.

Another way of describing a synaptic conductance is to use the expression $s = s_{\max}(t/\tau_s)\exp(1 - t/\tau_s)$ for the conductance after a presynaptic action potential that occurs at time $t = 0$. This expression is called an alpha function, and it starts at zero, reaches its peak value $s_{\max}$ at $t = \tau_s$, and then decays with a time constant τ_s. To determine s for a sequence of action potentials in this case, we integrate the equation

$$\tau_s \frac{ds}{dt} = e s_{\exp} - s\,, \quad \text{where} \quad \tau_s \frac{ds_{\exp}}{dt} = -s_{\exp} \tag{5.47}$$

and the update rule applied immediately after a presynaptic action potential is $s_{\exp} \rightarrow s_{\exp} + s_{\max}$.

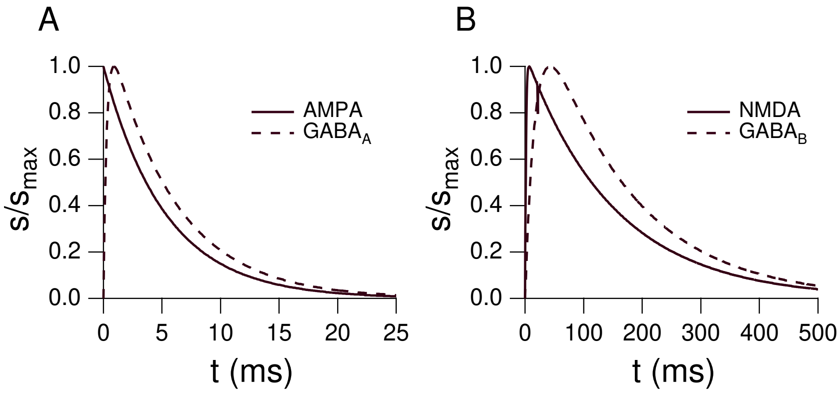

Figure 5.23: Time-dependent conductances fit to match AMPA, $\mathrm{GABA_A}$, $\mathrm{GABA_B}$, and NMDA synaptic conductances. A) The AMPA curve is a single exponential described by equation 5.43 with $\tau_s = 5.26$ ms. The $\mathrm{GABA_A}$ curve is a difference of exponentials with $\tau_1 = 5.6$ ms and $\tau_{\mathrm{rise}} = 0.3$ ms. B) Both curves are differences of two exponentials. The NMDA curve has $\tau_1 = 152$ ms and $\tau_{\mathrm{rise}} = 1.5$ ms, and the $\mathrm{GABA_B}$ curve has $\tau_1 = 150$ ms and $\tau_{\mathrm{rise}} = 20$ ms.

A Sampling of Synaptic Conductances

Synapses can exert their effects on the soma, dendrites, axon spike-initiation zone, or presynaptic terminals of their postsynaptic targets. There are two broad classes of synaptic conductances that are distinguished by whether the transmitter binds directly to the synaptic channel and activates it, or the transmitter binds to a distinct receptor that activates the conductance indirectly through an intracellular second-messenger signaling pathway. The first class is called ionotropic and the second metabotropic. Ionotropic synaptic conductances activate and deactivate more rapidly than metabotropic conductances. Metabotropic receptors can, in addition to opening channels, cause fundamental and long-lasting changes inside a neuron. In addition, the second messenger cascade can act as a chemical amplifier.

Glutamate and GABA (γ-aminobutyric acid) are the major excitatory and inhibitory transmitters in the brain. Both act ionotropically and metabotropically. The principal ionotropic receptor types for glutamate are called AMPA and NMDA after chemicals (agonists) that simulate the effects of the natural transmitter glutamate. Both AMPA and NMDA receptors produce mixed-cation conductances with reversal potentials around 0 mV. The AMPA current is fast activating and deactivating (figure 5.23A). The NMDA receptor is somewhat slower to activate and deactivates considerably more slowly (figure 5.23B). In addition, NMDA receptors have a novel voltage dependence. The current due to the NMDA receptor has an additional factor that depends on the postsynaptic potential. It can be written as $\overline{g}_{\mathrm{NMDA}} s G_{\mathrm{NMDA}}(V)(V-E)$. The factor $G_{\mathrm{NMDA}}(V)$ describes an extra voltage dependence due to the fact that, when the postsynaptic neuron is near its resting potential, NMDA receptors are blocked by Mg^{2+} ions. To activate the conductance, the postsynaptic neuron must be depolarized to knock out the blocking ions. Jahr and Stevens (1990) have fit this dependence by (figure 5.24)

$$G_{\text{NMDA}} = \left(1 + \frac{[\text{Mg}^{2+}]}{3.57\ \text{mM}} \exp(V/16.13\ \text{mV})\right)^{-1} . \tag{5.48}$$

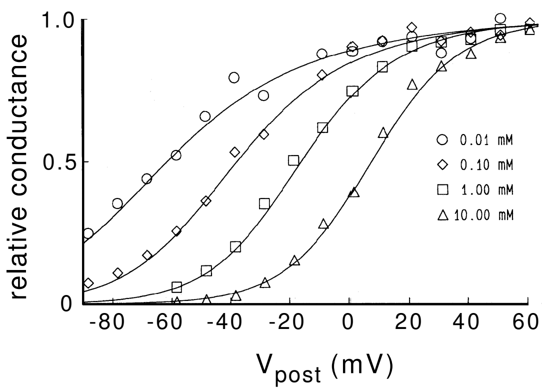

Figure 5.24: Dependence of the NMDA conductance on the extracellular Mg^{2+} concentration. Normal extracellular Mg^{2+} concentrations are in the range of 1 to 2 mM. The relative conductance plotted is the factor G_{NMDA} in equation 5.48. (Adapted from Jahr and Stevens, 1990)

NMDA receptors conduct Ca^{2+} ions as well as monovalent cations. Entry of Ca^{2+} ions through NMDA receptors is a critical event for long-term modification of synaptic strength at many synapses. The fact that conduction through NMDA receptors requires both pre- and postsynaptic depolarization means that the Ca^{2+} entry that induces synaptic modification acts as a coincidence detector of pre- and postsynaptic activity. This plays an important role in connection with the Hebb rule for synaptic modification discussed in chapter 8.

Two important inhibitory synaptic conductances in the brain are both activated by the neurotransmitter GABA (γ-aminobutyric acid). GABA_A receptors produce relatively fast ionotropic Cl^- conductances (figure 5.23A). GABA_B conductances are metabotropic and are slower and longer lasting K^+ conductances (figure 5.23B).

Neurons have a large number of metabotropic receptors that bind many different neurotransmitters and neuromodulators including glutamate, serotonin, dopamine, norepinephrine, and acetylcholine. These have a wide variety of effects and exert an enormous influence on the functioning of the nervous system (see Harris-Warrick and Marder, 1991).

Some synapses release transmitter due to depolarization of the synaptic terminal even if no action potentials are fired. For such transmission, s_∞ can vary as a graded function of the presynaptic potential. In addition to chemical synapses, neurons can be coupled through electrical synapses (gap junctions) that produce a synaptic current proportional to the difference between the pre- and postsynaptic membrane potentials,

$$I_{\mathrm{s}} = \overline{g}_{\mathrm{s}}(V_{post} - V_{pre})\,. \tag{5.49}$$

Some gap junctions rectify so that positive and negative current flow is not equal for potential differences of the same magnitude.

Release Probability and Short-Term Plasticity

The magnitude of the conductance change produced in a postsynaptic neuron by a presynaptic action potential can depend on the history of activity at the synapse. The effects of activity on synaptic conductances are termed short- and long-term depending on the length of time that they persist. Short-term plasticity refers to a number of phenomena that affect the probability that a presynaptic action potential opens postsynaptic channels and that last anywhere from milliseconds to tens of seconds. The effects of long-term plasticity are extremely persistent, lasting, for example, as long as the preparation being studied can be kept alive. The modeling and implications of long-term plasticity are considered in chapter 8. Here we describe how short-term synaptic plasticity can be described mathematically. The models we discuss have been applied in a variety of cases including neuromuscular junctions (Magleby, 1987) and neocortical synapses (Varela *et al*, 1997; Markram *et al*, 1997).

Figure 5.25 illustrates two principal types of short-term plasticity, depression and facilitation. Figure 5.25A shows postsynaptic current pulses produced in one cortical pyramidal neuron by evoking a series of action potentials in another pyramidal neuron presynaptic to the first. The pulses decrease in amplitude dramatically upon repeated activation of the synaptic conductance, revealing short-term synaptic depression. Figure 5.25B shows a similar series of postsynaptic current pulses recorded in a cortical inhibitory interneuron when a sequence of action potentials was evoked in a presynaptic pyramidal cell. In this case, the amplitude of the pulses increases, and thus the synapse facilitates. In general, synapses can exhibit facilitation and depression over a variety of time scales, and multiple components of short-term plasticity can be found at the same synapse. To keep the discussion simple, we consider synapses that exhibit either facilitation or depression, but not both.

Facilitation and depression are thought to reflect presynaptic processes that modify the probability of transmitter release. In both cases, the release probability after a long period of presynaptic silence is $P_{\mathrm{rel}} = P_0$. Activity at the synapse causes P_{rel} to increase in the case of facilitation and to decrease for depression. Between presynaptic action potentials, the release

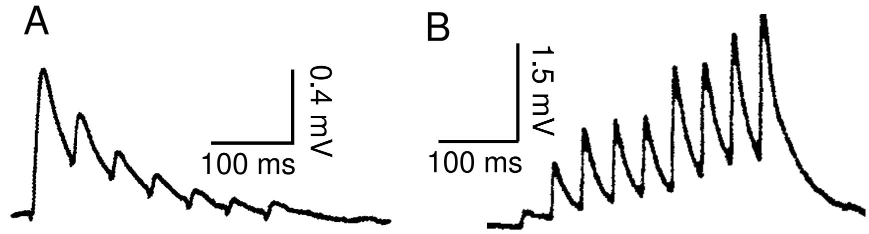

Figure 5.25: Depression and facilitation of excitatory intracortical synapses. A) Depression of an excitatory synapse between two layer 5 pyramidal cells recorded in a slice of rat somatosensory cortex. Spikes were evoked by current injection into the presynaptic neuron and postsynaptic currents were recorded with a second electrode. B) Facilitation of an excitatory synapse from a pyramidal neuron to an inhibitory interneuron in layer 2/3 of rat somatosensory cortex. (From Markram *et al*, 1997)

probability decays exponentially back to its 'resting' value P_0,

$$\tau_{\mathrm{P}} \frac{dP_{\mathrm{rel}}}{dt} = P_0 - P_{\mathrm{rel}} \, . \tag{5.50}$$

The parameter τ_{P} controls the rate at which the release probability decays to P_0.

The models of facilitation and depression differ in how the release probability is changed by presynaptic activity. In the case of facilitation, P_{rel} is augmented by making the replacement $P_{\mathrm{rel}} \to P_{\mathrm{rel}} + f_{\mathrm{F}}(1 - P_{\mathrm{rel}})$ immediately after a presynaptic action potential. The parameter f_{F} (with $f_{\mathrm{F}} \geq 0$) controls the degree of facilitation, and the factor $(1 - P_{\mathrm{rel}})$ prevents the release probability from growing larger than one. To model depression, the release probability is reduced after a presynaptic action potential by making the replacement $P_{\mathrm{rel}} \to f_{\mathrm{D}} P_{\mathrm{rel}}$. In this case, the parameter f_{D} (with $0 \leq f_{\mathrm{D}} \leq 1$) controls the amount of depression, and the factor P_{rel} prevents the release probability from becoming negative.

We begin by analyzing the effects of facilitation on synaptic transmission for a presynaptic spike train with Poisson statistics. In particular, we compute the average steady-state release probability, denoted by $\langle P_{\mathrm{rel}} \rangle$. The steady-state value of $\langle P_{\mathrm{rel}} \rangle$ is determined by requiring that the facilitation that occurs after each presynaptic action potential is exactly canceled by the average exponential decrement that occurs between presynaptic spikes. Consider two presynaptic action potentials separated by an interval τ, and suppose that the release probability takes its average value value $\langle P_{\mathrm{rel}} \rangle$ at the time of the first spike. Immediately after this spike, it is augmented to $\langle P_{\mathrm{rel}} \rangle + f_{\mathrm{F}}(1 - \langle P_{\mathrm{rel}} \rangle)$. By the time of the second spike, this will have decayed to $P_0 + (\langle P_{\mathrm{rel}} \rangle + f_{\mathrm{F}}(1 - \langle P_{\mathrm{rel}} \rangle) - P_0) \exp(-\tau/\tau_{\mathrm{P}})$, which is obtained by integrating equation 5.50. The average value of the exponential decay factor in this expression is the integral over all positive τ values of $\exp(-\tau/\tau_{\mathrm{P}})$ times the probability density for a Poisson spike train with a firing rate r to produce an interspike interval of duration τ, which is $r\exp(-r\tau)$ (see chapter 1). Thus, the average exponential decrement is

$$r\int_0^\infty d\tau\ \exp(-r\tau - \tau/\tau_P) = \frac{r\tau_P}{1+r\tau_P}\,. \qquad (5.51)$$

In order for the release probability to return, on average, to its steady-state value between presynaptic spikes, we must therefore require that

$$\langle P_{rel}\rangle = P_0 + \left(\langle P_{rel}\rangle + f_F(1-\langle P_{rel}\rangle) - P_0\right)\frac{r\tau_P}{1+r\tau_P}\,. \qquad (5.52)$$

Solving for $\langle P_{rel}\rangle$ gives

$$\langle P_{rel}\rangle = \frac{P_0 + f_F r\tau_P}{1+rf_F\tau_P}\,. \qquad (5.53)$$

This equals P_0 at low rates and rises toward the value one at high rates (figure 5.26A). As a result, isolated spikes in low-frequency trains are transmitted with lower probability than spikes occurring within high-frequency bursts (Lisman, 1997). The synaptic transmission rate when the presynaptic neuron is firing at rate r is the firing rate times the release probability. This grows quadratically as a function of r for small rates and approaches r at high rates (figure 5.26A).

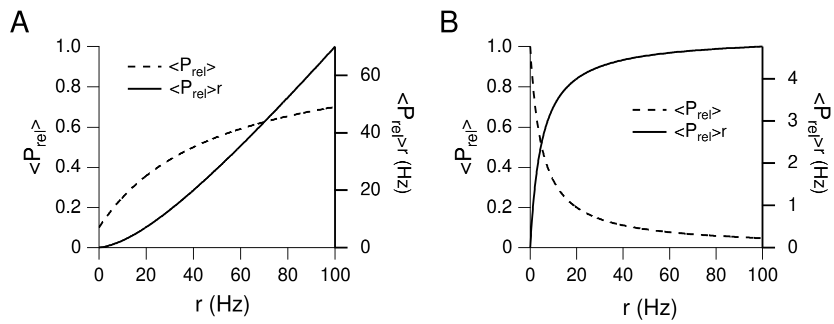

Figure 5.26: The effects of facilitation and depression on synaptic transmission. A) Release probability and transmission rate for a facilitating synapse as a function of the firing rate of a Poisson presynaptic spike train. The dashed curve shows the rise of the average steady-state release probability as the presynaptic rate increases. The solid curve is the average rate of transmission, which is the average release probability times the presynaptic firing rate. The parameters of the model were $P_0 = 0.1$, $f_F = 0.4$, and $\tau_P = 50$ ms. B) Same as A, but for the case of depression. The parameters of the model were $P_0 = 1$, $f_D = 0.4$, and $\tau_P = 500$ ms.

The steady-state value of $\langle P_{rel}\rangle$ for a Poisson presynaptic spike train can also be computed in the case of depression. The only difference from the above derivation is that following a presynaptic spike $\langle P_{rel}\rangle$ is decreased to $f_D\langle P_{rel}\rangle$. Thus, the consistency condition 5.52 is replaced by

$$\langle P_{rel}\rangle = P_0 + (f_D\langle P_{rel}\rangle - P_0)\frac{r\tau_P}{1+r\tau_P} \qquad (5.54)$$

giving

$$\langle P_{\mathrm{rel}} \rangle = \frac{P_0}{1 + (1 - f_{\mathrm{D}}) r \tau_{\mathrm{P}}} \tag{5.55}$$

This equals P_0 at low rates and goes to zero as $1/r$ at high rates (figure 5.26B), which has some interesting consequences. As noted above, the average rate of vesicle release, and thus the average rate of successful synaptic transmissions is equal to $\langle P_{\mathrm{rel}} \rangle$ times the presynaptic rate r. Because $\langle P_{\mathrm{rel}} \rangle$ is proportional to $1/r$ at high rates, the average transmission rate is independent of r in this range. This can be seen by the flattening of the solid curve in figure 5.26B. As a result, synapses that depress do not convey information about the values of high presynaptic firing rates to their postsynaptic targets. The presynaptic firing rate at which the transmission rate starts to become independent of r is around $1/((1 - f_{\mathrm{D}})\tau_{\mathrm{P}})$, which is in the range of 10 to 20 Hz for typical synaptic parameter values measured.

If depressing synapses do not convey information about firing rates, what do they convey? The equations given above only allowed us to compute the steady-state value of the average release probability. To answer this question, we need to study the dynamics of $\langle P_{\mathrm{rel}} \rangle$ in response to rapidly changing presynaptic firing rates. For time-dependent rates, the average release probability satisfies the equation

$$\tau_{\mathrm{P}} \frac{d\langle P_{\mathrm{rel}} \rangle}{dt} = P_0 - \langle P_{\mathrm{rel}} \rangle - (1 - f_{\mathrm{D}}) \tau_{\mathrm{P}} r \langle P_{\mathrm{rel}} \rangle \,. \tag{5.56}$$

This is obtained by combining equation 5.50 with the rule for decrement of the release probability following a presynaptic spike. Note that for constant r, the steady-state solution of this equation, obtained by setting both sides to zero, is equal to the result in equation 5.55.

Figure 5.27 shows the result of solving equation 5.56 for a series of steps in the presynaptic firing rate. The average transmission rate, $\langle P_{\mathrm{rel}} \rangle r$ is plotted in this figure. Note first that the transmission rates during the 25, 100, 10 and 40 Hz periods are quite similar. This is a consequence of the $1/r$ dependence of the average release probability, as discussed above. The largest transmission rates in the figure occur during the sharp upward transitions between different presynaptic rates. This illustrates the important point that depressing synapses amplify transient signals relative to steady-state inputs. The transients corresponding the 25 to 100 Hz transition and the 10 to 40 Hz transition are of roughly equal amplitudes, but the transient for the 10 to 40 Hz transition is broader than that for the 20 to 100 Hz transition.

The equality of amplitudes of the two upward transients in figure 5.27 is another consequence of the $1/r$ behavior of $\langle P_{\mathrm{rel}} \rangle$. Suppose that the presynaptic firing rate makes a sudden transition from a steady value r to a new value $r + \Delta r$. Before the transition, the average release probability is given by equation 5.55. Immediately after the transition, before the release probability has had time to adjust to the new input rate, the average transmission rate will be this previous value of $\langle P_{\mathrm{rel}} \rangle$ times the new rate $r + \Delta r$, which is $P_0(r + \Delta r)/(1 + (1 - f_{\mathrm{D}})r\tau_{\mathrm{P}})$. For sufficiently high rates, this is approximately proportional to $(r + \Delta r)/r$. The size of the change in the transmission rate is thus proportional to $\Delta r/r$, which means that depressing synapses not only amplify transient inputs, they transmit them in a logarithmically compressed manner. The amplitude of the transient transmission rate is proportional to the fractional change, not the absolute change, in the presynaptic firing rate. The two transients seen in figure 5.27 have similar amplitudes because in both cases $\Delta r/r = 3$. The difference in the recovery time for the two upward transients in figure 5.27 is due to the fact that the effective time constant governing the recovery to a new steady-state level r in equation 5.56 is $\tau_{\mathrm{P}}/(1 + (1 - f_{\mathrm{D}})\tau_{\mathrm{P}} r$.

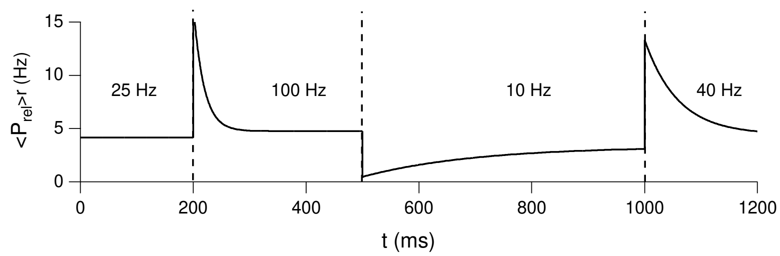

Figure 5.27: The average rate of transmission for a synapse with depression when the presynaptic firing rate changes in a sequence of steps. The firing rates are held constant at the values 25, 100, 10 and 40 Hz, except for abrupt changes at the times indicated by the dashed lines. The parameters of the model were $P_0 = 1$, $f_{\mathrm{D}} = 0.6$, and $\tau_{\mathrm{P}} = 500$ ms.

The transmission of presynaptic action potentials across a synapse with short-term plasticity represents a dynamic recoding of the information contained in the presynaptic spike train. Facilitation at synapses accentuates clusters and bursts of spikes over isolated spikes and tends to remove negative correlations from the presynaptic spike train. Depression of synaptic transmission amplifies transients and recodes them so the information about the fractional rather than absolute magnitude of the change in presynaptic rate is transmitted. This has the additional effect of removing positive correlations from the presynaptic spike train.

Modeling Channels

In previous sections, we described the Hodgkin-Huxley formalism for describing voltage-dependent conductances arising from a large number of channels. With the advent of single channel studies, microscopic descriptions of the transitions between the conformational states of channel molecules have been developed. Because these models describe complex molecules, they typically involve many states and transitions. Here, we discuss simple versions of these models that capture the spirit of single channel modeling without getting mired down in the details.

Models of single channels are based on state diagrams that indicate the possible conformational states that a channel can assume and provide rates for transitions between these states. Channel models can be constructed directly from these diagrams simply by keeping track of the state of the channel, and allowing it to change stochastically. If the model is updated in short time steps of duration Δt, the probability that the channel makes a given transition during an update interval is the appropriate transition rate times Δt. Simulating such transitions involves the same methods used to generate spike sequences characterized by a firing rate discussed in chapter 1. One of the states in the state diagram is designated as open and ion-conducting. The open probability P in such a model is one whenever this state is occupied and zero otherwise, and the current conducted by the channel is $\overline{g}P(V - E)$, where E is the appropriate reversal potential, and $\overline{g}$ is, in this case, the single channel open conductance.

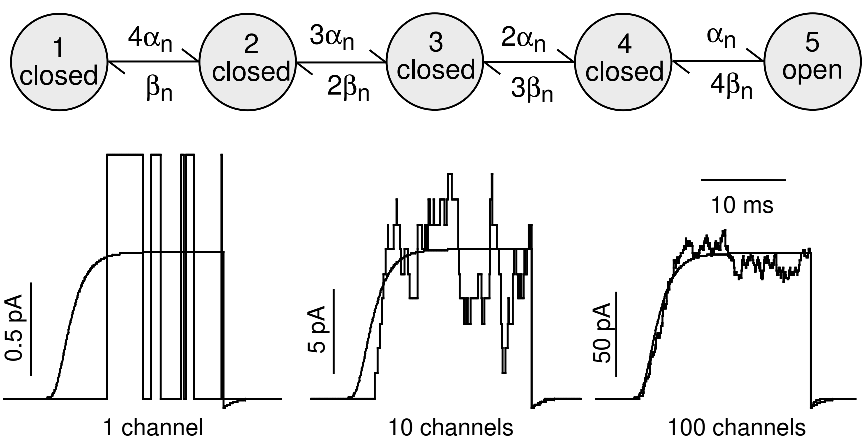

Figure 5.28: A model of the delayed-rectifier K^+ channel. The upper diagram shows the states and transition rates of the model. In the simulations shown in the lower panels, the membrane potential was initially held at -100 mV, then held at 10 mV for 20 ms, and finally returned to a holding potential of -100 mV. The smooth curves in these panels show the membrane current predicted by the Hodgkin-Huxley model in this situation. The left panel shows a simulation of a single channel that opened several times during the depolarization. The middle panel shows the total current from 10 simulated channels and the right panel corresponds to 100 channels. As the number of channels increases, the Hodgkin-Huxley model provides a more accurate description of the current.

Figure 5.28 shows the state diagram and simulation results of a model of a single delayed-rectifier K^+ channel that is closely related to the Hodgkin-Huxley description of the macroscopic delayed-rectifier conductance. The factors α_n and β_n in the transition rates shown in the state diagram of figure 5.28 are the voltage-dependent rate functions of the Hodgkin-Huxley model of the K^+ channel. We can think of state 1 in this diagram as a state in which all the subunits are closed. States 2, 3, 4, and 5 have 1, 2, 3, and 4 open subunits respectively. The factors of 1, 2, 3, and 4 in the transition rates correspond to the number of subunits that can make a given transition. The lower panels in figure 5.28 show simulations of this model involving 1, 10, and 100 channels. The sum of currents from all of these channels is compared with the current predicted by the Hodgkin-Huxley model (scaled with the appropriate maximal conductance). For each channel, the pattern of opening and closing is random, but when enough channels are simulated, the total current matches that of the Hodgkin-Huxley model quite well.

To see formally how the channel model in figure 5.28 reproduces the results of the Hodgkin-Huxley model when the currents from many channels are summed, we must consider a probabilistic description of this model. We denote the probability that a channel is in state a of figure 5.28 by p_a. Dynamic equations for these probabilities are easily derived by setting the rate of change for a given p_a equal to the probability per unit time of entry into state a from other states minus the rate for leaving the state. The entry probability per unit time is the product of the appropriate transition rate times the probability that the state making the transition is occupied. The probability per unit time for leaving is p_a times the sum of all the rates for possible transitions out of the state. Following this reasoning, the equations for the state probabilities are

$$\begin{aligned}
\frac{dp_1}{dt} &= \beta_n p_2 - 4\alpha_n p_1 \\
\frac{dp_2}{dt} &= 4\alpha_n p_1 + 2\beta_n p_3 - (\beta_n + 3\alpha_n) p_2 \\
\frac{dp_3}{dt} &= 3\alpha_n p_2 + 3\beta_n p_4 - (2\beta_n + 2\alpha_n) p_3 \\
\frac{dp_4}{dt} &= 2\alpha_n p_3 + 4\beta_n p_5 - (3\beta_n + \alpha_n) p_4 \\
\frac{dp_5}{dt} &= \alpha_n p_4 - 4\beta_n p_5 \,.
\end{aligned} \tag{5.57}$$

A solution for these equations can be constructed if we recall that n is the probability of a subunit being in the open state and $1 - n$ the probability of it being closed. State 1 has 4 closed subunits and thus $p_1 = (1-n)^4$. State 5, the open state, has 4 open subunits so $p_5 = n^4 = P$. State 2 has one open subunit, which can be any one of the four subunits, and three closed states making $p_2 = 4n(1-n)^3$. Similar arguments yield $p_3 = 6n^2(1-n)^2$ and $p_4 = 4n^3(1-n)$. These expressions generate a solution to the above equations provided that n satisfies equation 5.30 (exercise 7). If the initial values of the p_a's differ from the pattern predicted by this solution, these differences will decay to zero with a time constant of order τ_n.

In the Hodgkin-Huxley model of the Na^+ conductance, the activation and inactivation processes are assumed to act independently. The schematic in figure 5.18B, which cartoons the mechanism believed to be responsible for inactivation, suggests that this assumption is incorrect. The ball that inactivates the channel is located inside the cell membrane where it cannot be affected directly by the potential across the membrane. Furthermore, in this scheme, the ball cannot occupy the channel pore until the activation gate has opened, making the two processes interdependent. The sigmoidal form of the inactivation rate function $\beta_h(V)$ also suggests that something is wrong with the Hodgkin-Huxley description of the inactivation process. In fact $\beta_h(V)$ has a shape very similar to the asymptotic activation function $m_\infty(V)$ suggesting that the inactivation rate should really depend on the state of activation m, rather than on V (see Marom and Abbott, 1994).

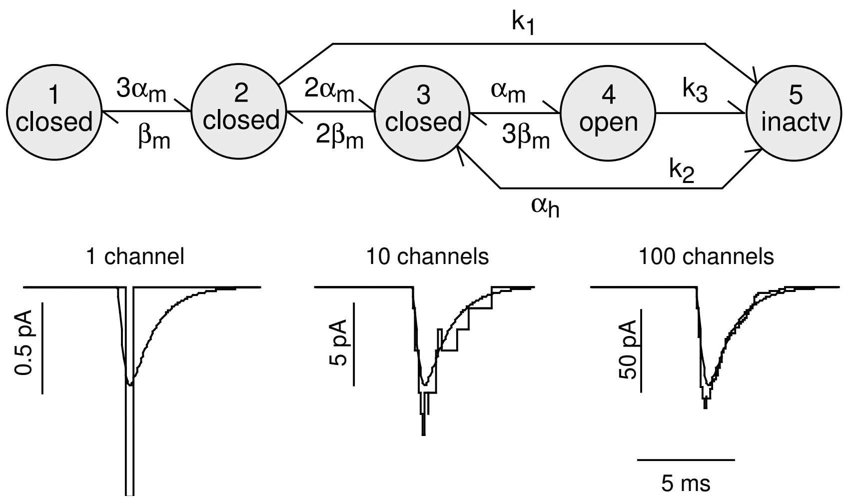

Figure 5.29: A model of the fast Na^+ channel. The upper diagram shows the states and transitions rates of the model. The values $k_1 = 0.24$/ms, $k_2 = 0.4$/ms, and $k_1 = 1.5$/ms were used in the simulations shown in the lower panels in which the membrane potential was initially held at -100 mV, then held at 10 mV for 20 ms, and finally returned to a holding potential of -100 mV. The smooth curves in these panels show the membrane current predicted by the Hodgkin-Huxley model in this situation. The left panel shows a simulation of a single channel that opened once during the depolarization. The middle panel shows the total current from 10 simulated channels and the right panel corresponds to 100 channels. As the number of channels increases, the Hodgkin-Huxley model provides a fairly accurate description of the current, but it is not identical to the channel model in this case.

Work on Na^+ channel models supports this view, and the state diagram in figure 5.29 reflects this by having a state-dependent, voltage-independent inactivation mechanism. This diagram is a simplified version of a Na^+ channel model due to Patlak (1991). The sequence of transitions that lead to channel opening through states 1,2,3, and 4 is identical to that of the Hodgkin-Huxley model with transition rates determined by the Hodgkin-Huxley functions $\alpha_\mathrm{m}(V)$ and $\beta_\mathrm{m}(V)$ and appropriate combinatoric factors. The transition to the inactivated state 5, however, is quite different from the inactivation process in the Hodgkin-Huxley model. The transition rates k_1, k_2, and k_3 are constants, independent of voltage, and inactivation transitions can only occur from states 2, 3, and 4. The deinactivation process occurs at the Hodgkin-Huxley rate $\beta_h(V)$ from state 5 to state 3.

Figure 5.29 shows simulations of this Na^+ channel model. In contrast to the K^+ channel model shown in figure 5.28, this model does not reproduce exactly the results of the Hodgkin-Huxley model when large numbers of channels are summed. Nevertheless, the two models agree quite well, as seen in the lower right panel of figure 5.29. The agreement, despite the different mechanisms of inactivation, is due to the speed of the activation process for the Na^+ conductance. The activation variable m of the Hodgkin-Huxley model reaches its voltage-dependent asymptotic value $m_\infty(V)$ so rapidly that it is difficult to distinguish inactivation processes that depend on m from those that depend on voltage. Differences between the two models are only apparent during a sub-millisecond time period while the conductance is activating. Experiments that can resolve this time scale support the channel model over the original Hodgkin-Huxley description (see exercise 9).

5.5 Further Reading and References

Further Reading

Braitenberg, V & Schuz, A (1991) *Anatomy of the Cortex*. Berlin:Springer-Verlag.

Harris-Warrick, RM & Marder E (1991) Modulation of neural networks for behavior. *Annual Review of Neuroscience* **14**:39-47.

Hille, B (1992) *Ionic Channels of Excitable Membranes*. Sunderland, MA:Sinauer Association.

Hodgkin, AL & Huxley, AF (1952) A quantitative description of membrane current and its application to conduction and excitation in nerve. *Journal of Physiology (London)* **117**:500-544.

Jack, JJB, Noble, D & Tsien, RW (1975) *Electrical Current Flow in Excitable Cells*. Oxford:Oxford University Press.

Johnston, D & Wu, SM (1995) *Foundations of Cellular Neurophysiology*. Cambridge, MA:MIT Press.

Kandel, ER & Schwartz, eds. (1985) *Principles of Neural Science, 2nd ed*. New York:Elsevier.

Kandel, ER, Schwartz, JH & Jessel, TM (1991), eds. *Principles of Neural Science, 3rd ed*. New York:Elsevier.

Koch, C (1998) *Biophysics of Computation: Information Processing in Single Neurons*. New York:Oxford University Press.

Koch, C & Segev, I, editors (1998) *Methods in Neuronal Modeling: From Synapses to Networks*. Cambridge, MA:MIT Press.

Magleby, KL (1987) Short-term changes in synaptic efficacy. In: G Edelman, W Gall & W Cowan, editors, *Synaptic Function*. New York:John Wiley & Sons, pp 21-56.

Rall, W (1977) Core conductor theory and cable properties of neurons. In ER Kandel, editor, *Handbook of Physiology, Volume 1*. Bethesda:American Physiological Society, 39-97.

Sakmann, B & Neher, E (1983) *Single Channel Recording*. New York:Plenum.

Tuckwell, HC (1988) *Introduction to Theoretical Neurobiology*. Cambridge, UK:Cambridge University Press.

Zucker, RS (1989). Short-term synaptic plasticity. *Annual Review of Neuroscience* **12**:13-31.

References

Abbott, LF (1992) Simple diagrammatic rules for solving dendritic cable problems. *Physica* **A185**:343-356.

Abbott, LF, Varela, JA, Sen, K & Nelson, SB (1997) Synaptic depression and cortical gain control. *Science* **275**:220-224.

Bean, BP (1981) Sodium channel inactivation in the crayfish giant axon: Must channels open before inactivating? *Biophysical Journal* **35**:595-614.

Butz, EG & Cowan, JD (1974) Transient potentials in dendritic systems of arbitrary geometry. *Biophysical Journal* **14**:661-689.

Destexhe, A, Mainen, Z & Sejnowkski, T (1994) Synthesis of models for excitable membranes, synaptic transmission and neuromodulation using a common kinetic formalism. *Journal of Computational Neuroscience* **1**:195-230.

Haberly, LB (1990) Olfactory cortex. In GM Shepherd, editor, *The Synaptic Organization of the Brain*. New York:Oxford University Press.

Holmes, WR (1986) A continuous cable method for determining the transient potential in passive trees of known geometry. *Biological Cybernetics* **55**:115-124.

Jahr, CE & Stevens, CF (1990) A quantitative description of NMDA receptor channel kinetic behavior. *Journal of Neuroscience* **10**:1830-1837.

Koch, C & Poggio, T (1985) A simple algorithm for solving the cable equation in dendritic trees of arbitrary geometry. *Journal of Neuroscience Methods* **12**:303-315.

Lisman, JE (1997) Bursts as a unit of neural information: making unreliable synapses reliable. *Trends in Neuroscience* **20**:38-43.

Markram, H, Wang, Y & Tsodyks, MV (1998) Differential signalling via the same axon of neocortical pyramidal neurons. *Proceedings of the National Academy of Science USA* **95**:5323-5328.

Marom, S & Abbott, LF (1994) Modeling state-dependent inactivation of membrane currents. *Biophysical Journal* **67**:515-520.

Patlak, J (1991) Molecular kinetics of voltage-dependent Na^+channels. *Physiological Reviews* **71**:1047-1080.

Rall, W (1959) Branching dendritic trees and motoneuron membrane resistivity. *Experimental Neurology* **2**:503-532.

Stuart, GJ & Sakmann, B (1994) Active propagation of somatic action potentials into neocortical pyramidal cell dendrites. *Nature* **367**:69-72.

Stuart, GJ & Spruston, N (1998) Determinants of voltage attenuation in neocortical pyramidal neuron dendrites. *Journal of Neuroscience* **18**:3501-3510.

Tsai, KY, Carnevale, NT, Claiborne, BJ & Brown, TH (1994) Efficient mapping from neuroanatomical to electrotonic space. *Network* **5**:21-46.

Tsodyks, MV & Markram, H (1997) The neural code between neocortical pyramidal neurons depends on neurotransmitter release probability. *Proceedings of the National Academy of Science USA* **94**:719-723.

Varela, J, Sen, K, Gibson, J, Fost, J, Abbott, LF, Nelson, SB (1997) A quantitative description of short-term plasticity at excitatory synapses in layer 2/3 of rat primary visual cortex. *Journal of Neuroscience* **17**:7926-7940.

Zador, A, Agmon-Snir, H & Segev, I (1995) The morphoelectric transform: A graphical approach to dendritic function. *Journal of Neuroscience* **15**:1669-1682.

5.6 Exercises

1. Show that equation 5.15 is the solution to the cable equation along an infinite cable in response to the injected current $i_e = I_e \delta(t)\delta(x)/2\pi a$.

2. Verify that the solution for an isolated junction given by equations 5.17 and 5.18 satisfies the correct boundary conditions at the junction point $x_1 = x_2 = x_3 = 0$.

3. Generalize the solution for an isolated junction of equation 5.17 to the time-dependent case when the injected current on segment 2 is $i_e = I_e \delta(t)\delta(x_2 - y)/2\pi a$

4. Show that the expression for $v(x)$ given in figure 5.11, with R_1 and R_2 given by equations 5.19 and 5.20, satisfies the cable equation and the boundary conditions $v(0) = v_{\text{soma}}$ and $\partial v/\partial x = 0$ when $x = L$.

5. Show that the expression for $v(x)$ given in figure 5.13, with R_3 and R_4 given by equations 5.22 and 5.23, satisfies the cable equation and the boundary conditions $v(0) = 0$ and $\partial v/\partial x = 0$ when $x = L$.

6. The Nernst equation was derived in this chapter under the assumption that the membrane potential was negative and the ion being considered was positively charged. Rederive the Nernst equation, 5.26, for a negatively charged ion and for the case when E is positive to verify that it applies in all these cases.

7. Compute the value of the release probability P_{rel} at the time of each presynaptic spike for a regular, periodic, constant-frequency presynaptic spike train as a function of the presynaptic firing rate. Do this for both the depression and facilitation models discussed in the text.

8. Verify that the state probabilities listed after equation 5.57 are actually a solution of these equations if n satisfies equation 5.30.

9. Construct and simulate the K^+ channel model of figure 5.28. Plot the mean squared deviation between the current produced by N such model channels and the Hodgkin-Huxley current as a function of N, matching the amplitude of the Hodgkin-Huxley model so that the mean currents are the same.

10. Construct and simulate the Na^+ channel model of figure 5.29. Compare the current through 100 such channels with the current predicted by the Hodgkin-Huxley model at very short times after a step-like depolarization of the membrane potential. What are the differences and why do they occur?